

Acoustic Leak Monitoring in Black Liquor Recovery Boilers

A study commissioned by the Finnish Recovery Boiler Committee and conducted at the Laboratory of Machine Dynamics, Tampere University of Technology.

Juha Miettinen
Ville Järvinen
Robert Hildebrand

Tampere 13.06.2005

Abstract:

The present study seeks to analyze the feasibility of detecting water and steam leaks in black liquor recovery boilers, since such leaks represent both safety hazards and economic losses. Water leaks in the bottom wall, in particular, involve a risk of explosion as water mixes with the sodium metal of the smelt. This justifies the heavy emphasis in this report on bottom wall water leaks, while addressing the detection of steam leaks more expediently.

The hypothesis presented in this work is that the attenuation of the structure-borne sound from a water leak, through the bottom wall, to the sensor, may be so strong at the high frequencies often monitored, that it is undetectable above the background noise level. Thus, the present work provides a detailed study of that attenuation, both analytical and experimental.

The steam leak problem, and particularly the size of leaks that are detectable, is addressed by using scaling laws from the theory of flow-induced sound, and inferring scaling factors from previously published works on this topic.

1 Introduction

The present study considers the feasibility of detecting water and steam leaks in black liquor recovery boilers, using vibroacoustic monitoring. Vibroacoustic monitoring may take the form of either the continuous measurement of structure-borne sound (primarily in the bottom wall, to detect *water* leaks) or of airborne sound (primarily to detect *steam* leaks). As such, the study is not primarily concerned with the specific instrumentation, transducers or signal processing required of a monitoring system. Rather, it is concerned with the physical acoustics problem of how the sound and vibration fields generated by a leak propagate in the structure or in the gases inside the furnace. That propagation, and in particular the resulting strength of the leak-induced vibroacoustic field at the monitoring positions, in relation to the background noise level induced by operation, dictates whether or not detection is feasible at all, whatever the details of the monitoring system.

Steam and water leaks are of interest for both safety and economic reasons.

The main safety consideration is the risk of an explosion, should water enter the smelt, which mainly consists of sodium metal. That risk is particularly great when the leak involves water, rather than steam, and even more so if it is in the bottom wall. Thus, the topic of water leaks in the bottom wall is given the greatest share of the attention in this work.

Current practice, in monitoring for water leaks in the bottom wall, is to use acoustic emission sensors, which are most sensitive at very high frequencies (say, 150 kHz). Reportedly, however, that methodology is not completely satisfactory. The hypothesis presented in this work is that the signal-to-noise ratio at such frequencies may often be inadequate to detect a leak, especially due to the strong attenuation of the structure-borne sound from the leak as it crosses the periodic fin-tube structure of the boiler's bottom wall. The attenuation is a function of frequency, depending on the periodicity of the wall, and the damping due to the smelt and other mechanisms. Typically, one expects a large attenuation at high frequencies, which makes the risk of a poor signal-to-noise ratio especially acute, given that the monitored frequencies are very high. The present work provides a detailed study of that attenuation, both analytical and experimental, which is found in section 2 below, and which bears out the hypothesis that the attenuation is high at the monitored frequencies.

Steam leak detection by microphones is also treated, in section 3 below. However, in keeping with the intent to emphasize water leaks, the approach to steam leaks has been to merely supply some new interpretation to already existing results from the literature, rather than undertake extensive new theoretical or experimental work. Scaling laws from the theory of flow-induced sound are used, and the needed scaling factors are inferred from previously published results. A preliminary conclusion is that 1.4 mm leaks are about the lower limit of what can be detected inside the furnace, but that conclusion is based on very imprecisely reported input data.

2 Water leaks in the bottom wall

The problem is illustrated in figure 1.

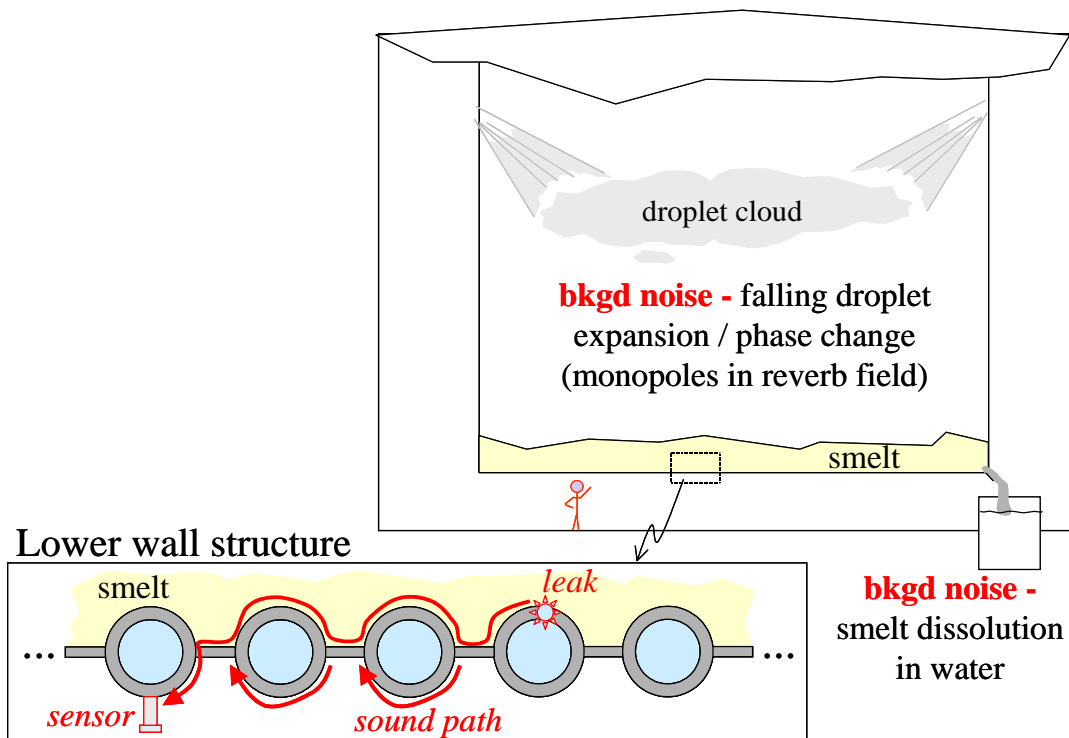


Figure 1. Vibroacoustic sources and paths in the recovery boiler. All sources, except for a water leak (or cracking leading to such a leak) are regarded as background noise. The inset shows the structure of the bottom wall, in which tube and plate (“fin”) elements alternate.

Vibrations are induced in the bottom wall of the boiler from combustion of black liquor droplets, smelt dissolution, and other sources which are present in normal operation. These vibrations are referred to as “background noise”, since they are undesirable disturbances that are registered by the transducers monitoring for water leaks.

Should metal cracking or a water leak occur, it might also generate vibrations at a specific point (illustrated in the inset of the figure). These vibrations then spread throughout the bottom wall, eventually reaching one of the transducers of the measurement system.

The hypothesis guiding the present work is that the signal-to-noise ratio may be too weak at the sensor; i.e., leakage-induced vibrations may be too weak, as compared to operation-induced vibrations. That ratio depends on the following factors:

- attenuation (decay of vibrations with distance in the wall)
- background vibration levels
- vibratory power input of the leakage mechanism into the structure

The first of those factors, *attenuation*, is investigated in this report by a computational model (section 2.1 below) and by field measurements in actual recovery boilers (section 2.2 below). The second factor, *background noise*, is also investigated in the field measurements (section 2.2 below),

but its computational modeling has not been possible within the scope of this project (although recommendations for such work are presented). The third factor, *power input*, is not investigated here, but recommended for future investigation. Because the attenuation is expected to be greatest in the direction across the pipes, the following work concentrates on the attenuation of plane waves in that direction.

2.1 Theoretical study

The structure of the bottom wall has the character of a periodic structure, of the form ... – fin – tube – fin – tube – fin – ...etc., as illustrated in figure 2.

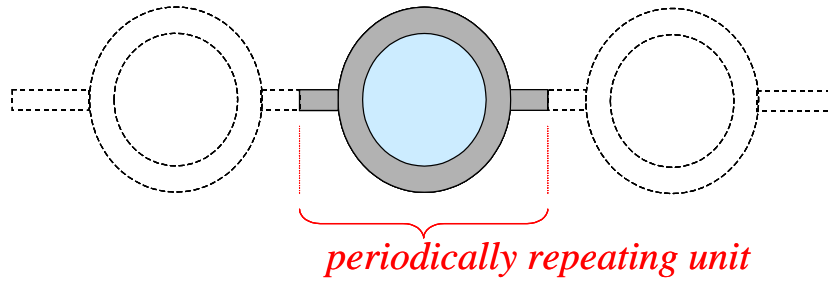


Figure 2. Periodic structure of the bottom wall, and its periodically repeating unit: half fin – tube – half fin.

Although the structure does, of course, have boundaries, it may be well-approximated as *infinite* periodic, since its dimensions are very large with respect to the relevant wavelengths. The greater the decay and the higher the frequency, the better that approximation will be (for greater decay, reflections from the boundaries are much weaker than the direct field from a water leak; for higher frequencies, the wavelength becomes ever shorter with respect to the large dimensions of the gross structure). In that respect, it is similar to a railway track or a ship's hull with its regularly repeating lateral stiffeners, for example.

Infinite periodic structures tend to show marked pass-band and stop-band behavior, i.e., regions of attenuation minima and maxima, respectively. Moreover, they lend themselves to relatively efficient analysis, since the dynamics of the gross structure may be constructed from the dynamics of the periodically repeating unit, and the computational effort may therefore be focused on the latter.

2.1.1 Basic formulation

Material damping in the structure is accounted for by allowing complex Young's moduli

$$E_f = E_{f,nom}(1 + i\eta_f) \text{ and } E_t = E_{t,nom}(1 + i\eta_t), \quad (2.1)$$

for the fin and tube materials, where $E_{f,nom}$ and $E_{t,nom}$ are the respective real-valued Young's moduli (as would be found in a handbook), and η_f and η_t are the loss factors. All other forms of damping in the structure (such as friction at welds, etc.) are incorporated into these loss factors as well.

As a first approximation (which is then modified in the following sections), both the fin and the tube are modeled as *thin plates*. Thus, rotational inertia and shear deformation are ignored in the treatment of bending, and the curvature of the tube is ignored. Both of these approximations are

unsatisfactory in the frequency range of interest, but will facilitate the initial development. Thus, the bending stiffnesses are

$$D_f = \frac{E_f h_f^3}{12(1-\nu_f^2)}, \quad (2.2)$$

and

$$D_t = \frac{E_t h_t^3}{12(1-\nu_t^2)} \quad (2.3)$$

of the fin and tube, respectively, where h the thickness, E the Young's modulus, and ν the Poisson's ratio, each subscripted with either f for the fin or t for the tube. The bending wave numbers are

$$k_{Bf} = \sqrt[4]{\frac{\rho_f h_f}{D_f} \omega^2}, \text{ and } k_{Bt} = \sqrt[4]{\frac{\rho_t h_t}{D_t} \omega^2}, \quad (2.4)$$

of the fin and tube, respectively, where ρ is the density, $\omega = 2\pi f$ is the circular frequency in rad/s and f the frequency in Hz. The quasi-longitudinal wave numbers are

$$k_{Lf} = \omega \sqrt{\frac{\rho_f (1-\nu_f)}{E_f}}, \text{ and } k_{Lt} = \omega \sqrt{\frac{\rho_t (1-\nu_t)}{E_t}}, \quad (2.5)$$

of the fin and tube, respectively, which is the appropriate form for a plate [Cremer et.al., 1988].

The displacements in fin and the tube of the repeating unit are first identified, using the coordinate systems identified in figure 3.

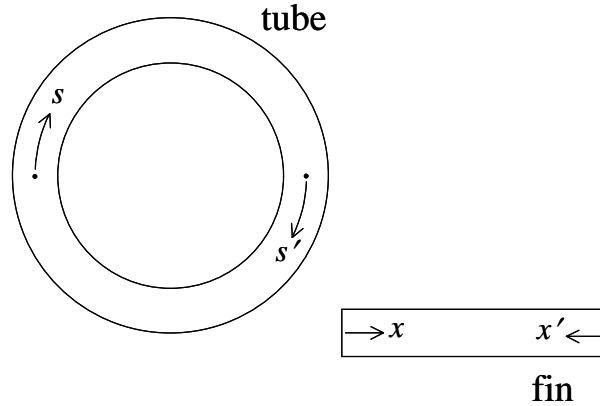


Figure 3. Coordinate systems for tube and fin, respectively. Note that $s' = s - \pi R$, and $x' = x - L$.

The horizontal and vertical displacements are indicated by u and v , respectively. Subscripts are used in the pattern pq . The first subscript indicates whether the displacement refers to the fin ($p = "f"$) or to the tube ($p = "t"$). The second subscript, if present, indicates whether the displacement refers to the left side of the repeating unit ($q = "l"$), or to the right side ($q = "r"$).

For the tube,

$$u_t(s) = B_{tr} e^{ik_{Bt}s'} + N_{tr} e^{k_{Bt}s'} + B_{tl} e^{-ik_{Bt}s} + N_{tl} e^{-k_{Bt}s}, \quad 0 \leq s < \pi R \quad (2.6)$$

$$u_t(s) = B_{ur}e^{-ik_{Br}s'} + N_{ur}e^{-k_{Br}s'} + B_{ul}e^{ik_{Br}s} + N_{ul}e^{k_{Br}s}, \pi R \leq s < 2\pi R \text{ (i.e., } 0 \leq s' < \pi R) \quad (2.7)$$

$$v_t(s) = L_{tr}e^{ik_{Lr}s'} + L_{tl}e^{-ik_{Lr}s}, 0 \leq s < \pi R \quad (2.8)$$

$$v_t(s) = L_{ur}e^{-ik_{Lr}s'} + L_{ul}e^{ik_{Lr}s}, \pi R \leq s < 2\pi R \text{ (i.e., } 0 \leq s' < \pi R) \quad (2.9)$$

where $s' = s - \pi R$.

For the fin to the right of the tube,

$$u_{fr}(x) = L_{fr}e^{-ik_{Lr}x} + e^{-g}L_{fl}e^{ik_{Lr}x'}, \quad (2.10)$$

$$v_{fr}(x) = B_{fr}e^{-ik_{Br}x} + N_{fr}e^{-k_{Br}x} + e^{-g}B_{fl}e^{ik_{Br}x'} + e^{-g}N_{fl}e^{k_{Br}x'}. \quad (2.11)$$

where $x' = x - L$, and for the fin to the left of the tube,

$$u_{fl}(x) = L_{fl}e^{ik_{Lr}x'} + e^g L_{fr}e^{-ik_{Lr}x}, \quad (2.12)$$

$$v_{fl}(x) = B_{fl}e^{ik_{Br}x'} + N_{fl}e^{k_{Br}x'} + e^{-g}B_{fr}e^{-ik_{Br}x} + e^g N_{fr}e^{-k_{Br}x}. \quad (2.13)$$

The Floquet condition has been used here to account for the repeating unit being part of an infinite periodic structure; it states that the vibrations of a repeating unit are the same as those of the unit to its left, modified only by the factor e^{-g} , where the ‘‘propagation constant’’ g is complex. The real part of g represents attenuation per unit (decay occurring as one moves to the right if $a \equiv \text{Re}(g)$ is positive), and the imaginary part represents a phase shift.

Attention is now focused on the two junctions of the fin to the tube that occur in each of the repeating units. Here the various displacement terms of the tube and the fin are interpreted as waves and nearfields, and the fin-tube junctions as representing local transmission-reflection problems for those wave fields and near fields. This is illustrated in figure 4.

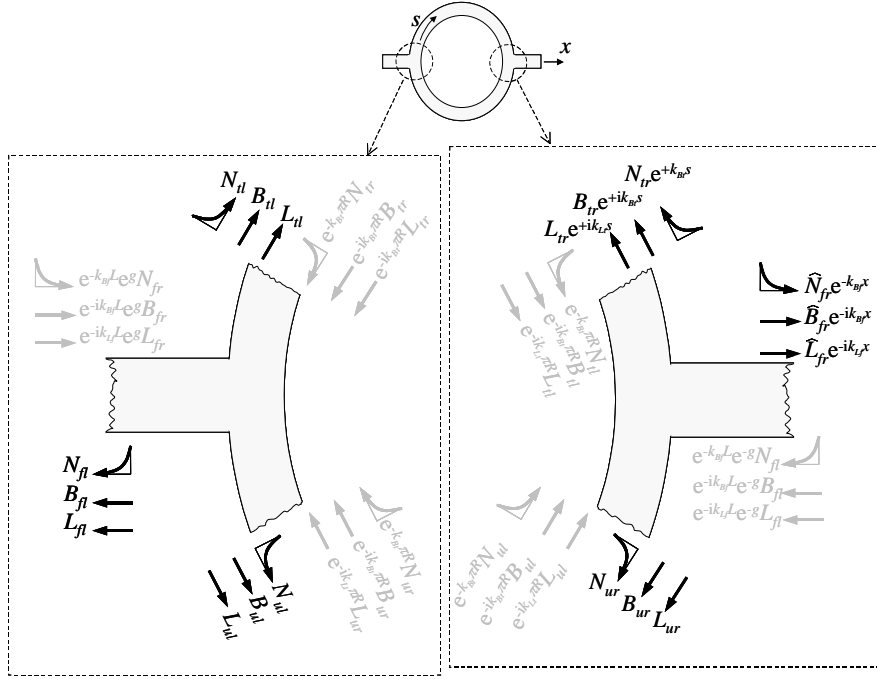


Figure 4. Waves and nearfields at the left and right tube-fin junctions of a repeating unit.

Conditions of kinematical continuity within the tube (across a junction), and between the tube and the fin (“connectedness”), as well as equilibrium, must apply at each of the two junctions. Exactly 18 such conditions can be identified, corresponding to the 18 independent wave and nearfield amplitudes. These are given in the following, and evidently constitute an eigenvalue problem for the propagation constant g :

Connectedness of **vertical displacement** at **right** junction (fin-tube):

$$B_{fr} + N_{fr} + e^{-ik_{Bf}L} e^{-g} B_{fl} + e^{-k_{Bf}L} e^{-g} N_{fl} = -L_{tr} - e^{-ik_{Lr}\pi R} L_{tl} \quad (2.14 a)$$

Continuity of **vertical displacement** at **right** junction (within tube):

$$L_{tr} + e^{-ik_{Lr}\pi R} L_{tl} = L_{ur} + e^{-ik_{Lr}\pi R} L_{ul} \quad (2.14 b)$$

Connectedness of **vertical displacement** at **left** junction (fin-tube):

$$B_{fl} + N_{fl} + e^{-ik_{Bf}L} e^g B_{fr} + e^{-k_{Bf}L} e^g N_{fr} = L_{tl} + e^{-ik_{Lr}\pi R} L_{tr} \quad (2.14 c)$$

Continuity of **vertical displacement** at **left** junction (within tube):

$$L_{tl} + e^{-ik_{Lr}\pi R} L_{tr} = L_{ul} + e^{-ik_{Lr}\pi R} L_{ur} \quad (2.14 d)$$

Connectedness of **horizontal displacement** at **right** junction (fin-tube):

$$L_{fr} + e^{-ik_{Lf}L} e^{-g} L_{fl} = B_{tr} + N_{tr} + e^{-ik_{Bt}\pi R} B_{tl} + e^{-k_{Bt}\pi R} N_{tl} \quad (2.14 e)$$

Continuity of **horizontal displacement** at **right** junction (within tube):

$$B_{tr} + N_{tr} + e^{-ik_{Bt}\pi R} B_{tl} + e^{-k_{Bt}\pi R} N_{tl} = B_{ur} + N_{ur} + e^{-ik_{Bt}\pi R} B_{ul} + e^{-k_{Bt}\pi R} N_{ul} \quad (2.14 f)$$

Connectedness of **horizontal displacement** at **left** junction (fin-tube):

$$L_{fl} + e^{-ik_{Lf}L} e^g L_{fr} = -B_{tl} - N_{tl} - e^{-ik_{Bt}\pi R} B_{tr} - e^{-k_{Bt}\pi R} N_{tr} \quad (2.14 g)$$

Continuity of **horizontal displacement** at **left** junction (within tube):

$$B_{tl} + N_{tl} + e^{-ik_{Bt}\pi R} B_{tr} + e^{-k_{Bt}\pi R} N_{tr} = B_{ul} + N_{ul} + e^{-ik_{Bt}\pi R} B_{ur} + e^{-k_{Bt}\pi R} N_{ur} \quad (2.14 h)$$

Connectedness of **angular displacement** at **right** junction (fin-tube):

$$\begin{aligned} & -ik_{Bf} B_{fr} - k_{Bf} N_{fr} + ik_{Bf} e^{-ik_{Bf}L} e^{-g} B_{fl} + k_{Bf} e^{-k_{Bf}L} e^{-g} N_{fl} \\ & = ik_{Bt} B_{tr} + k_{Bt} N_{tr} - ik_{Bt} e^{-ik_{Bt}\pi R} B_{tl} - k_{Bt} e^{-k_{Bt}\pi R} N_{tl} \end{aligned} \quad (2.14 i)$$

Continuity of **angular displacement** at **right** junction (within tube):

$$\begin{aligned} & ik_{Bt} B_{tr} + k_{Bt} N_{tr} - ik_{Bt} e^{-ik_{Bt}\pi R} B_{tl} - k_{Bt} e^{-k_{Bt}\pi R} N_{tl} \\ & = -ik_{Bt} B_{ur} - k_{Bt} N_{ur} + ik_{Bt} e^{-ik_{Bt}\pi R} B_{ul} + k_{Bt} e^{-k_{Bt}\pi R} N_{ul} \end{aligned} \quad (2.14 j)$$

Connectedness of **angular displacement** at **left** junction (fin-tube):

$$\begin{aligned} & ik_{Bf} B_{fl} + k_{Bf} N_{fl} - ik_{Bf} e^{-ik_{Bf}L} e^g B_{fr} - k_{Bf} e^{-k_{Bf}L} e^g N_{fr} \\ & = -ik_{Bt} B_{tl} - k_{Bt} N_{tl} + ik_{Bt} e^{-ik_{Bt}\pi R} B_{tr} + k_{Bt} e^{-k_{Bt}\pi R} N_{tr} \end{aligned} \quad (2.14 k)$$

Continuity of **angular displacement** at **left** junction (within tube):

$$\begin{aligned} & -ik_{Bt} B_{tl} - k_{Bt} N_{tl} + ik_{Bt} e^{-ik_{Bt}\pi R} B_{tr} + k_{Bt} e^{-k_{Bt}\pi R} N_{tr} \\ & = ik_{Bt} B_{ul} + k_{Bt} N_{ul} - ik_{Bt} e^{-ik_{Bt}\pi R} B_{ur} - k_{Bt} e^{-k_{Bt}\pi R} N_{ur} \end{aligned} \quad (2.14 l)$$

Equilibrium of **vertical forces** at **right** junction:

$$\begin{aligned} & D_f \left(ik_{Bf}^3 B_{fr} - k_{Bf}^3 N_{fr} - ik_{Bf}^3 e^{-ik_{Bf}L} e^{-g} B_{fl} + k_{Bf}^3 e^{-k_{Bf}L} e^{-g} N_{fl} \right) \\ & = E_t h_t \left(ik_{Lt} L_{tr} - ik_{Lt} e^{-ik_{Lt}\pi R} L_{tl} \right) - E_t h_t \left(ik_{Lt} L_{ur} - ik_{Lt} e^{-ik_{Lt}\pi R} L_{ul} \right) \end{aligned} \quad (2.14 m)$$

Equilibrium of **vertical forces** at **left** junction:

$$\begin{aligned} & D_f \left(-ik_{Bf}^3 B_{fl} + k_{Bf}^3 N_{fl} + ik_{Bf}^3 e^{-ik_{Bf}L} e^g B_{fr} - k_{Bf}^3 e^{-k_{Bf}L} e^g N_{fr} \right) \\ & = -E_t h_t \left(-ik_{Lt} L_{tl} + ik_{Lt} e^{-ik_{Lt}\pi R} L_{tr} \right) + E_t h_t \left(ik_{Lt} L_{ul} - ik_{Lt} e^{-ik_{Lt}\pi R} L_{ur} \right) \end{aligned} \quad (2.14 n)$$

Equilibrium of **horizontal forces** at **right** junction:

$$\begin{aligned} & E_f h_f \left(-ik_{Lf} L_{fr} + ik_{Lf} e^{-ik_{Lf}L} e^{-g} L_{fl} \right) \\ & = -D_t \left(-ik_{Bt}^3 B_{tr} + k_{Bt}^3 N_{tr} + ik_{Bt}^3 e^{-ik_{Bt}\pi R} B_{tl} - k_{Bt}^3 e^{-k_{Bt}\pi R} N_{tl} \right) \\ & \quad + D_t \left(ik_{Bt}^3 B_{ur} - k_{Bt}^3 N_{ur} - ik_{Bt}^3 e^{-ik_{Bt}\pi R} B_{ul} + k_{Bt}^3 e^{-k_{Bt}\pi R} N_{ul} \right) \end{aligned} \quad (2.14 o)$$

Equilibrium of **horizontal forces** at **left** junction:

$$\begin{aligned} & E_f h_f \left(ik_{Lf} L_{fl} - ik_{Lf} e^{-ik_{Lf}L} e^g L_{fr} \right) \\ & = -D_t \left(ik_{Bt}^3 B_{tl} - k_{Bt}^3 N_{tl} - ik_{Bt}^3 e^{-ik_{Bt}\pi R} B_{tr} + k_{Bt}^3 e^{-k_{Bt}\pi R} N_{tr} \right) \\ & \quad + D_t \left(-ik_{Bt}^3 B_{ul} + k_{Bt}^3 N_{ul} + ik_{Bt}^3 e^{-ik_{Bt}\pi R} B_{ur} - k_{Bt}^3 e^{-k_{Bt}\pi R} N_{ur} \right) \end{aligned} \quad (2.14 p)$$

Equilibrium of **rotational moments** at **right** junction:

$$\begin{aligned}
& D_f \left(-k_{Bf}^2 B_{fr} + k_{Bf}^2 N_{fr} - k_{Bf}^2 e^{-ik_{Bf}L} e^{-g} B_{fl} + k_{Bf}^2 e^{-k_{Bf}L} e^{-g} N_{fl} \right) \\
& = D_t \left(-k_{Bt}^2 B_{tr} + k_{Bt}^2 N_{tr} - k_{Bt}^2 e^{-ik_{Bt}\pi R} B_{tl} + k_{Bt}^2 e^{-k_{Bt}\pi R} N_{tl} \right) \\
& \quad - D_t \left(-k_{Bt}^2 B_{ur} + k_{Bt}^2 N_{ur} - k_{Bt}^2 e^{-ik_{Bt}\pi R} B_{ul} + k_{Bt}^2 e^{-k_{Bt}\pi R} N_{ul} \right)
\end{aligned} \tag{2.14 q}$$

Equilibrium of **rotational moments** at **left** junction:

$$\begin{aligned}
& D_f \left(-k_{Bf}^2 B_{fl} + k_{Bf}^2 N_{fl} - k_{Bf}^2 e^{-ik_{Bf}L} e^g B_{fr} + k_{Bf}^2 e^{-k_{Bf}L} e^g N_{fr} \right) \\
& = D_t \left(-k_{Bt}^2 B_{tl} + k_{Bt}^2 N_{tl} - k_{Bt}^2 e^{-ik_{Bt}\pi R} B_{tr} + k_{Bt}^2 e^{-k_{Bt}\pi R} N_{tr} \right) \\
& \quad - D_t \left(-k_{Bt}^2 B_{ul} + k_{Bt}^2 N_{ul} - k_{Bt}^2 e^{-ik_{Bt}\pi R} B_{ur} + k_{Bt}^2 e^{-k_{Bt}\pi R} N_{ur} \right)
\end{aligned} \tag{2.14 r}$$

Define a vector \mathbf{u} containing all of the unknown wave and nearfield amplitudes:

$$\begin{aligned}
\mathbf{u} &= [u_1 \quad u_2 \quad \dots \quad u_{18}]^T \\
&= [L_{fr} \quad B_{fr} \quad N_{fr} \quad L_{tr} \quad B_{tr} \quad N_{tr} \quad L_{ur} \quad B_{ur} \quad N_{ur} \\
& \quad L_{fl} \quad B_{fl} \quad N_{fl} \quad L_{tl} \quad B_{tl} \quad N_{tl} \quad L_{ul} \quad B_{ul} \quad N_{ul}]^T
\end{aligned} \tag{2.15}$$

Then define the matrix \mathbf{A} , which appears in the form of a table, below, with empty cells representing zeroes.

Table 1. Matrix \mathbf{A} defined.

1	2	3	4	5	6	7	8	9	10	11	12	13	14	15	16	17	18
	1	1	1							$\gamma_B e^g$	$\gamma_N e^g$	γ_L					
			1			-1						γ_L				- γ_L	
	$\gamma_B e^g$	$\gamma_N e^g$	- γ_L							1	1	-1					
			γ_L				- γ_L					1				-1	
1				-1	-1				$\gamma_L e^g$				- γ_B	- γ_N			
				1	1		-1	-1					γ_B	γ_N		- γ_B	- γ_N
$\gamma_L e^g$				γ_B	γ_N				1				1	1			
				γ_B	γ_N		- γ_B	- γ_N					1	1		-1	-1
	- ik_{Bf}	- k_{Bf}		- ik_{Bt}	- k_{Bt}					$ik_{Bf}\gamma_B e^g$	$k_{Bf}\gamma_N e^g$		$ik_{Bt}\gamma_B$	$k_{Bt}\gamma_N$			
				ik_{Bt}	k_{Bt}		ik_{Bt}	k_{Bt}					- $ik_{Bt}\gamma_B$	- $k_{Bt}\gamma_N$		- $ik_{Bt}\gamma_B$	- $k_{Bt}\gamma_N$
	- $ik_{Bf}\gamma_B e^g$	- $k_{Bf}\gamma_N e^g$		- $ik_{Bt}\gamma_B$	- $k_{Bt}\gamma_N$					ik_{Bf}	k_{Bf}		ik_{Bt}	k_{Bt}			
				$ik_{Bt}\gamma_B$	$k_{Bt}\gamma_N$		$ik_{Bt}\gamma_B$	$k_{Bt}\gamma_N$					- ik_{Bt}	- k_{Bt}		- ik_{Bt}	- k_{Bt}
	$ik_{Bf}^2 D_f$	$k_{Bf}^2 D_f$	- $ik_{L1} E_{h1}$				$ik_{L1} E_{h1}$						$ik_{L1} E_{h1} \gamma_{L1}$			- $ik_{L1} E_{h1} \gamma_{L1}$	
	$ik_{Bf}^2 D_f \gamma_{L1} e^g$	$k_{Bf}^2 D_f \gamma_{N1} e^g$	- $ik_{L1} E_{h1} \gamma_{L1}$				$ik_{L1} E_{h1} \gamma_{L1}$				- $ik_{Bf}^2 D_f$	$k_{Bf}^2 D_f$	- $ik_{L1} E_{h1}$			- $ik_{L1} E_{h1}$	
	- $ik_{L1} E_{h1}$			- $ik_{Bt}^2 D_t$	$k_{Bt}^2 D_t$		- $ik_{Bt}^2 D_t$	$k_{Bt}^2 D_t$	$ik_{L1} E_{h1} \gamma_{L1} e^g$				$ik_{Bt}^2 D_t \gamma_{Bt}$	- $k_{Bt}^2 D_t \gamma_{Nt}$		$ik_{Bt}^2 D_t \gamma_{Bt}$	- $k_{Bt}^2 D_t \gamma_{Nt}$
	- $ik_{L1} E_{h1} \gamma_{L1} e^g$			- $ik_{Bt}^2 D_t \gamma_{Bt}$	$k_{Bt}^2 D_t \gamma_{Nt}$		- $ik_{Bt}^2 D_t \gamma_{Bt}$	$k_{Bt}^2 D_t \gamma_{Nt}$	$ik_{L1} E_{h1} \gamma_{L1}$				$ik_{Bt}^2 D_t$	- $k_{Bt}^2 D_t$		$ik_{Bt}^2 D_t$	- $k_{Bt}^2 D_t$
	- $k_{Bf}^2 D_f$	$k_{Bf}^2 D_f$		$k_{Bt}^2 D_t$	- $k_{Bt}^2 D_t$		- $k_{Bt}^2 D_t$	$k_{Bt}^2 D_t$					$k_{Bt}^2 D_t \gamma_{Bt}$	- $k_{Bt}^2 D_t \gamma_{Nt}$		- $k_{Bt}^2 D_t \gamma_{Bt}$	$k_{Bt}^2 D_t \gamma_{Nt}$
	- $k_{Bf}^2 D_f \gamma_{L1} e^g$	$k_{Bf}^2 D_f \gamma_{N1} e^g$		$k_{Bt}^2 D_t \gamma_{Bt}$	- $k_{Bt}^2 D_t \gamma_{Nt}$		- $k_{Bt}^2 D_t \gamma_{Bt}$	$k_{Bt}^2 D_t \gamma_{Nt}$		- $k_{Bf}^2 D_f$	$k_{Bf}^2 D_f$		$k_{Bt}^2 D_t$	- $k_{Bt}^2 D_t$		- $k_{Bt}^2 D_t$	$k_{Bt}^2 D_t$

Solving the eigenvalue problem $\mathbf{A}\mathbf{u}=0$ gives the propagation constants g , and the attenuation constants are then $a = \text{Re}(g)$. The decay may also be expressed in decibels per unit as

$$d = 20 \log e^{-a} \text{ dB}, \tag{2.16}$$

or in decibels per meter as

$$d = 20 \log e^{-a/(L+2R)} \text{ dB}, \tag{2.17}$$

where L is the length of a fin and R radius of a tube (i.e., $L + 2R$ is the length of a repeating unit).

2.1.2 Thick plate corrections for the fin

The thin plate theory is not satisfactory at high frequencies, including most of the range of interest in the present application (say, above about 60 kHz). An approximate thick plate correction, but keeping the same formulation as above, is obtained by replacing the thin-plate bending wave numbers by thick-plate (Mindlin) bending wave numbers, and using an effective bending stiffness, reduced from that of the thin-plate theory. In fact, the approach used is not exactly the same as the Mindlin plate theory (the plate-theory analogous to Timoshenko beam theory), but an approximation of it, for two reasons.

The first reason is that the Mindlin plate theory has two bending wave numbers: a real one k_1 , analogous to the bending wave number k_B of the thin-plate theory, although $k_1 > k_B$; and, another one k_2 , which is imaginary at low frequencies, and real above some cut-on frequency. The second wave number, below the cut-on frequency, corresponds to the nearfields of the thin-plate theory (i.e., it gives $e^{\pm ik_2 x}$ terms corresponding to the $e^{\mp k_B x}$ terms of the thin-plate theory, since k_2 is imaginary). Although $|k_2| < |k_1|$ below the cut-on frequency, $|k_2| \approx |k_1|$ is a good approximation below about half of the cut-on frequency. Thus, in simply replacing k_B by k_1 in the matrix of the preceding section, the nearfield terms are replaced by $e^{\pm k_1 x} \approx e^{\mp ik_2 x}$.

The second reason is that the equations of continuity and equilibrium do not reflect the additional degrees-of-freedom introduced by allowing shear deformation as part of bending. The approximation made is to use the same set of equations, but to incorporate shear deformation by means of a reduced effective bending stiffness.

Abandoning the notation k_1 used for explanation above, the thick-plate bending wave number is given the same notation as the thin-plate wave numbers, but with an asterick “*”; it is:

$$k_{Bf*} = k_{1f} = \sqrt{\frac{\rho_f h_f}{2D_f} \left(\omega^2 \left[r_f^2 + \frac{D_f}{G_f t h_f} \right] + \sqrt{\omega^4 \left[r_f^2 + \frac{D_f}{G_f t h_f} \right]^2 - 4 \frac{D_f}{\rho_f h_f} \left[\omega^4 \frac{\rho_f r_f^2}{G_f \tau} - \omega^2 \right]} \right)}, \quad (2.18)$$

$$\approx -ik_{2f}$$

where $r_f = h_f / \sqrt{12}$ is the radius of gyration of the plate about its neutral axis, and $G_f = E_f / 2(1 + \nu_f)$ is the shear modulus.

The effective bending stiffness is then

$$D_{f*} = \left(\frac{k_{Bf*}}{k_{Bf}} \right)^4 D_f. \quad (2.19)$$

2.1.3 Curvature (shell) and thickness corrections for the tube

The corrections to account for tube curvature, and shear and rotational inertia (“thickness”, in the sense of needing a “thick shell” model), are made using the same strategy as for the thick-plate corrections for the fin. Rather than change the matrix A which was devised in 2.1.1 for thin plate models, it is more expedient to make use of effective wavenumbers, effective bending stiffness, and effective longitudinal stiffnesses.

The corrected wave numbers are found from the method of [Graff, 1970] for curved beams (and not repeated here), but replacing E for a beam (in Graff) by $E/(1 - \nu)$ to make it applicable to a plate, and using a radius of gyration $r_t = h_t/\sqrt{12}$ and “Timoshenko constant” $\tau = .83$. This approach is then applicable to plane waves propagating circumferentially on a thick, infinitely-long cylindrical shell. Note that both the “bending” and the “longitudinal” wave numbers are corrected in this case (their respective identifications as “bending” and “longitudinal” are only approximate, since each propagating mode now couples both in-plane and out-of-plane motions). These wave numbers are henceforth identified as k_{Bt^*} and k_{Lt^*} , and the adjusted bending stiffness and “effective” Young’s modulus are

$$D_{t^*} = \left(\frac{k_{Bt^*}}{k_{Bt}} \right)^4 D_t, \quad (2.20)$$

and

$$E_{t^*} = \left(\frac{k_{Lt^*}}{k_{Lt}} \right)^2 E_t \quad (2.21)$$

respectively.

2.1.4 Fluid interaction corrections: smelt and water

The method developed thusfar is adequate for the case of the boiler wall with unfilled-pipes and without a smelt layer having developed above it from boiler operation. Since it is the operating boiler that is of interest in continuous monitoring, however, the fluid-structure interactions involving the smelt and the water must also be included.

The smelt is difficult to include. Firstly, its properties (e.g., speed of sound, density, elastic properties, etc.) are little known. Secondly, it is not a fluid throughout the smelt layer; it is solidified near the wall and liquefied further away. Thirdly, as opposed to the situation in classical fluid-structure interaction problems, the smelt layer is not semi-infinite, but has a finite depth.

The water, although much better understood from the perspective of its properties, is nevertheless also problematic in that it is completely enclosed by the pipe, and represents a small volume (per unit length of a single pipe), so that its geometric distribution differs even more than that of the smelt from that of classical fluid-structure interaction problems.

All of the reservations stated above notwithstanding, the fluid interactions are nevertheless treated here as if they were classical (semi-infinite fluids). There are several reasons to believe that such a treatment is an adequate approximation, despite the reservations made. Firstly, the smelt properties

being so imperfectly known, additional approximation is not a serious drawback – the uncertainty from smelt properties will negate any possible benefit from a more complicated fluid model. Secondly, the solidified smelt layer is at a high temperature, and probably many orders of magnitude less stiff than the boiler wall material; pressure waves will be favorably radiated into it by the wall, while shear waves will not (because of the large impedance difference) – thus, it will effectively act as a fluid. Thirdly, and finally, the finiteness of the fluids becomes unimportant when the wavelength is small compared to the dimensions of the fluid volumes; that is the case above about 30 kHz (at which the ratio tube diameter-to-water wavelength is 1.27). Thus, the model can cover exactly that part of the frequency range of interest which the finite difference (2-d.o.f.) model, to be presented in section 2.1.5, will be inadequate for. Evidently, the approximation improves more and more as the frequency increases.

Physically, the fluids act as “added masses” (effective increases of the fin or tube density) below the so-called “coincidence frequency”, and as “radiation dampers” (effective increase of the loss factor of the fin or tube material) above that frequency. The coincidence frequency is distinct for each combination of fluid medium and structural element (solid medium); thus, there are three relevant coincidence frequencies in this problem: water-tube, smelt-tube, and smelt-fin (the combination water-fin obviously lacks any relevance, since the fin is never in contact with water). Let us call these f_{cwt} , f_{cst} , and f_{csf} respectively, and note that they occur when $k_{Bt^*} = k_{water} = \omega/c_{water}$, $k_{Bt^*} = k_{smelt} = \omega/c_{smelt}$, and $k_{Bf^*} = k_{smelt} = \omega/c_{smelt}$ respectively, where c_{smelt} is the speed of sound in the smelt and c_{water} the speed of sound in water.

For the fin, which only interacts with the smelt, the corrected wave number $k_{Bf^{**}}$ is calculated:

1. On $f > f_{csf}$, i.e., above coincidence, by the method of sections 2.1.1-2.1.2, but replacing the loss factor η_f by

$$\eta_{f^{**}} = \frac{\rho_{smelt} c_{smelt}}{\omega \rho_f h_f} \sqrt{\frac{1}{1 - f_{csf}/f}}, \quad (2.22)$$

[Cremer et.al., 1988], which accounts for the radiation damping effect.

2. On $f < f_{csf}$, i.e., below coincidence, as

$$k_{Bf^{**}} \approx k_{Bf^*} \left(1 + \frac{\rho_{smelt}}{\rho_f h_f (k_{Bf^*}^2 - k_{smelt}^2)^{1/2}} \right)^{1/4}, \quad (2.23)$$

[Junger – Feit, 1993], which accounts for the added mass effect.

For the tube, the assumption is made that $f_{cst} < f_{cwt}$; this will prove to be true for the particular properties assumed for the smelt in this work (see section 2.1.6). Then, the corrected wave number $k_{Bt^{**}}$ is calculated:

1. On $f > f_{cwt} > f_{cst}$, i.e., above both coincidences, by the method of sections 2.1.1-2.1.3, but replacing the loss factor η_t by

$$\eta_{t^{**}} = \frac{1}{\omega \rho_t h_t} \left(\rho_{smelt} c_{smelt} \sqrt{\frac{1}{1 - f_{cst}/f}} + \rho_{water} c_{water} \sqrt{\frac{1}{1 - f_{cwt}/f}} \right), \quad (2.24)$$

[Cremer et.al., 1988].

2. On $f_{cst} < f < f_{cwt}$, i.e., below water coincidence but above smelt coincidence, by the method of sections 2.1.1-2.1.3, but replacing the loss factor η_t by

$$\eta_{t^{**}} = \frac{\rho_{smelt} c_{smelt}}{\omega \rho_t h_t} \sqrt{\frac{1}{1 - f_{cst}/f}}, \quad (2.25)$$

[Cremer et.al., 1988], which accounts for radiation into the smelt, and then by multiplying the resulting wave number by the factor

$$\left(1 + \frac{\rho_{water}}{\rho_t h_t (k_{Bt^{**}}^2 - k_{water}^2)^{1/2}} \right)^{1/4}, \quad (2.26)$$

[Junger – Feit, 1993], which accounts for the added mass of the water.

3. On $f < f_{cst} < f_{cwt}$, i.e., below both coincidences, as

$$k_{Bt^{**}} \approx k_{Bt^*} \left(1 + \frac{\rho_{smelt}}{\rho_t h_t (k_{Bt^*}^2 - k_{smelt}^2)^{1/2}} \right)^{1/4} \left(1 + \frac{\rho_{water}}{\rho_t h_t (k_{Bt^*}^2 - k_{water}^2)^{1/2}} \right)^{1/4}. \quad (2.27)$$

The entire method then proceeds as in section 2.1.1, except that the uncorrected parameters:

k_{Bf} , k_{Lf} , k_{Bt} , k_{Lt} , D_f , E_f , η_f , D_t , E_t , and η_t ;

are replaced by the doubly-corrected ones (i.e., corrected for both thickness & curvature [1st *] and for fluid interactions [2nd *]):

$k_{Bf^{**}}$, $k_{Lf^{**}}$, $k_{Bt^{**}}$, $k_{Lt^{**}}$, D_f^{**} , E_f^{**} , η_f^{**} , D_t^{**} , E_t^{**} and η_t^{**} ,

respectively. Considering the valid range of the first approximation mentioned in section 2.1.2 (that $|k_2| \approx |k_1|$, reasonable up to the half cut-on frequency), and which is also applicable to the corrections of section 2.1.3, the entire method should be acceptable to about 200 kHz.

2.1.5 Two-d.o.f. finite difference model

At low frequencies, the 18-d.o.f. wave model described in sections 2.1.1 – 2.1.4 will not be valid, because the approximation that the small contained water volume can be regarded as semi-infinite, from the perspective of the tube, is not tenable. The bending wavelength, in that region, is of the order of, or larger than, the diameter of the enclosed water volume. Thus, another approach is needed. In this work, the frequency range 0-20 kHz has therefore been studied using a time-domain finite difference method, in which the fin and tube are simple lumped elements. The fin acts as a lumped stiffness, compliant for vertical and rotational relative motions of its opposite boundaries,

but rigid against horizontal motions (thus, only bending, not longitudinal, motions are now possible in the structure). The tube acts as a lumped inertial element. In vertical translations (horizontal ones are not allowed), the mass is that of the tube and the water, combined. In rotations, only the tube's rotational inertia is included; shear stresses are not transmitted across the tube-water interface. All damping is ignored.

The mass of the tube (including water) is

$$M_t = 2\pi R h_t \rho_t + \pi R^2 \rho_{water}. \quad (2.28)$$

The rotational inertial of the tube (without water) is

$$J_t = 2\pi R^3 h_t \rho_t. \quad (2.29)$$

The vertical translational stiffness of the fin is

$$K_f = \frac{12D_f}{L^3}. \quad (2.30)$$

The rotational stiffness of the fin is

$$K_{\theta f} = K_f \frac{d_{offset}^2}{2}, \quad (2.31)$$

where $d_{offset} = \frac{L^2}{6}$.

The bottom wall structure is thus modeled as a series of N repeating units as shown in figure 5, where N is large.

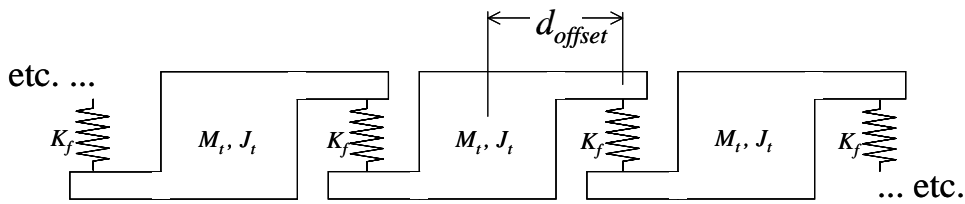


Figure 5. Schematic model of the bottom wall as a series of lumped elements. The fin represents a lumped stiffness, and the tube a lumped inertial element (in which the water only takes part in the translational motion).

Consider the tube of the j -th repeating unit in the series, counted from the left. Its motion is characterized by a vertical displacement v_j (positive upwards) and a rotation θ_j (positive counterclockwise). A free-body diagram of the tube is illustrated in figure 6, where the inertial forces are indicated by dashed arrows; dots indicate differentiation with respect to time.

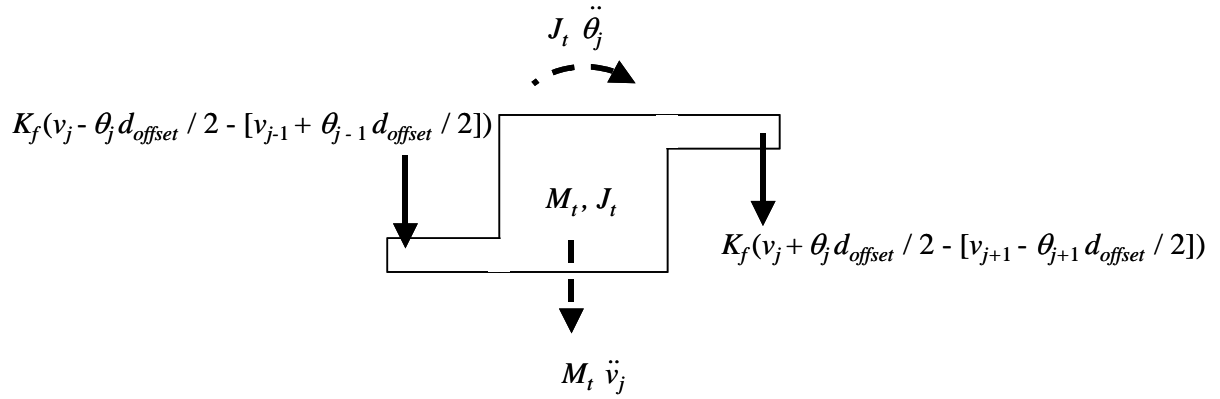


Figure 6. Free-body diagram of the tube of a single repeating unit. Inertial loads are given as dashed lines.

Conditions of vertical and rotational dynamic equilibrium then imply that

$$M_t \ddot{v}_j + K_f \left(2v_j - v_{j-1} - v_{j+1} + \theta_{j+1} \frac{d_{offset}}{2} - \theta_{j-1} \frac{d_{offset}}{2} \right) = 0, \quad (2.32)$$

and

$$J_t \ddot{\theta}_j + \frac{K_f d_{offset}}{2} \left(\theta_j d_{offset} + v_{j-1} - v_{j+1} + \theta_{j+1} \frac{d_{offset}}{2} + \theta_{j-1} \frac{d_{offset}}{2} \right) = 0. \quad (2.33)$$

Making the finite difference approximations of the time derivatives,

$$\ddot{v}_j \approx \frac{1}{\Delta t^2} (v_{j,new} - 2v_j + v_{j,old}), \quad (2.34)$$

and

$$\ddot{\theta}_j \approx \frac{1}{\Delta t^2} (\theta_{j,new} - 2\theta_j + \theta_{j,old}), \quad (2.35)$$

it is then possible to express each of the degrees-of-freedom at a “new” instant of time in terms of the d.o.f. at $j-1$, j , and $j+1$, at the two preceding instants “current” (Δt earlier) and “old” ($2\Delta t$ earlier), as

$$v_{j,new} = 2v_j - v_{j,old} - \frac{K_f \Delta t^2}{M_t} \left(2v_j - v_{j-1} - v_{j+1} + \theta_{j+1} \frac{d_{offset}}{2} - \theta_{j-1} \frac{d_{offset}}{2} \right) \quad (2.36)$$

and

$$\theta_{j,new} = 2\theta_j - \theta_{j,old} - \frac{K_f d_{offset} \Delta t^2}{2J_t} \left(\theta_j d_{offset} + v_{j-1} - v_{j+1} + \theta_{j+1} \frac{d_{offset}}{2} + \theta_{j-1} \frac{d_{offset}}{2} \right) \quad (2.37)$$

where the “current” instant of time is implied when no subscript is used.

The method then proceeds by specifying at rest initial conditions at all of the units,

$$v_j = v_{j,old} = \theta_j = \theta_{j,old} = 0, j \in [1, N]. \quad (2.38)$$

Next, the time is advanced by steps Δt , so that $t = m\Delta t$, as $m = 1, 2, 3 \dots$, while forcing the first unit in the series to undergo a harmonic oscillation of unit rotational amplitude at a frequency f (or rotational frequency $\omega = 2\pi f$) of interest,

$$\theta_{1,new} = \sin(2\pi ft), \quad (2.39)$$

and constraining all other degrees-of-freedom at the first and last (N -th) unit to be fixed

$$v_{1,new} = v_{N,new} = \theta_{N,new} = 0. \quad (2.40)$$

Evidently, using the equilibrium conditions expressed explicitly in terms of $v_{j,new}$ and $\theta_{j,new}$, for $j \in [2, N - 1]$, these d.o.f. can be solved in each step, knowing their values at all points in the preceding two time steps. That is possible for the entire time series, starting from the initial conditions, which supply two time instants.

Tracking the vertical displacement v_j at two units, $j = N_{ref}$ and $j = N_{resp}$, such that $N_{ref} \ll N_{resp} \ll N$, these may be filtered over a long time interval for their respective amplitudes $\hat{v}_{N_{ref}}(\omega)$ and $\hat{v}_{N_{resp}}(\omega)$ at the excitation frequency ω . The attenuation per unit is then

$$a(\omega) = -\frac{\log[\hat{v}_{resp}(\omega)/\hat{v}_{ref}(\omega)]}{\hat{v}_{resp}(\omega) - \hat{v}_{ref}(\omega)}. \quad (2.41)$$

The decay in decibels per unit is

$$d = 20 \log e^{-a} \text{ dB}, \quad (2.42)$$

and in decibels per meter is

$$d = 20 \log e^{-a/(L+2R)} \text{ dB}. \quad (2.43)$$

The procedure involved tonal filtering of v_j at frequency ω , because of the presence of other frequency components due to the initial transient. The first “ \ll ” condition above, $N_{ref} \ll N_{resp}$, ensures that the difference in amplitude is large enough to accurately find low attenuation levels, while the second “ \ll ” condition, $N_{resp} \ll N$, seeks to minimize the influence of reflections from the end of the finite series, since it gives the reflections an opportunity to attenuate before reaching N_{resp} .

2.1.6 Results

Input properties used to study the boiler are provided in table 2, below. The tube and fin materials have handbook values for steel. The loss factors, however, are selected to be .01 to account for losses at welds; [Cremer et.al., 1988] suggests that value for composite structures. The water also uses handbook values. The smelt density is estimated from [Kawaji et.al.] and [Adams], and the

speed of sound is a guess, based on the fact that in most fluids (including heavy metal fluids such as mercury) it falls in the 1200 – 1500 m/s range, tending towards the upper half of that range.

Table 2. Input parameters for the 18-dof wave theoretical model.

Material

Fin		
Young's modulus	$E_{f,nom}$	2.1×10^{11} N/m ²
Poisson's ratio	ν_f	0.3
Density	ρ_f	7800 kg/m ³
Loss factor	η_f	.01
Tube		
Young's modulus	$E_{t,nom}$	2.1×10^{11} N/m ²
Poisson's ratio	ν_t	0.3
Density	ρ_t	7800 kg/m ³
Loss factor	η_t	.01
Smelt		
Speed of sound	c_{smelt}	1400 m/s
Density	ρ_{smelt}	2000 kg/m ³
Water		
Speed of sound	c_{water}	1500 m/s
Density	ρ_{water}	1000 kg/m ³

Geometric

Fin thickness	h_f	.004 m
Fin length	L	.0127 m
Tube thickness	h_t	.00185 m
Tube radius	R	.03175 m

The finite difference model uses the same input parameters, as applicable. Moreover, the reference position, response position, and finite track length are, respectively,

$$N_{ref} = 2, N_{resp} = 40, \text{ and } N = 100.$$

Results, using the two models discussed above, are presented in figure 7. Since the finite difference model is suitable at low frequencies, and the wave model at high frequencies, the two results together nearly cover the entire range of interest 0 – 200 kHz.

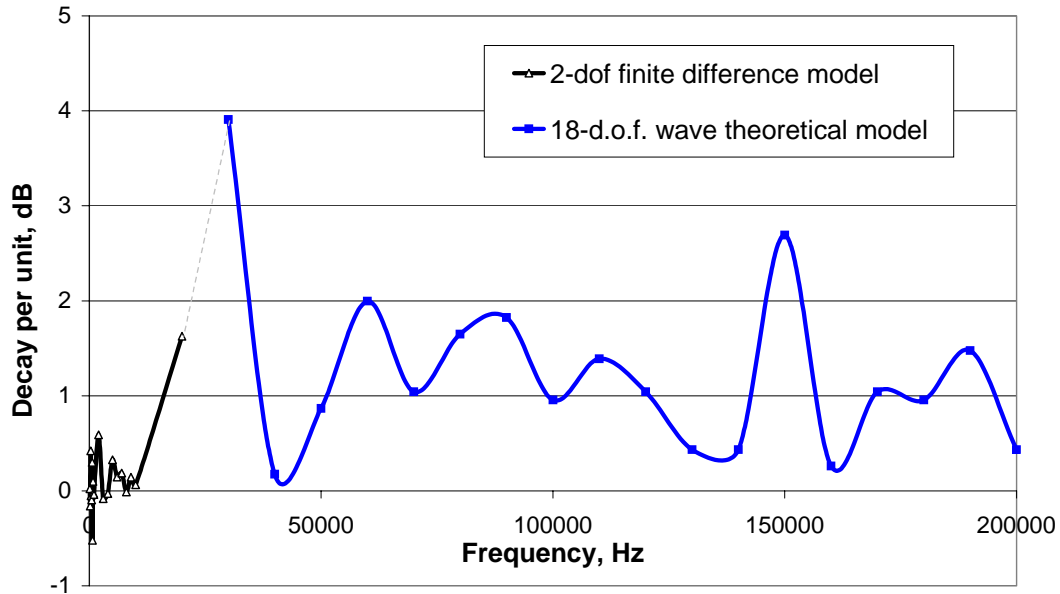


Figure 7. Predicted attenuation across the pipes of the bottom wall. Results at low frequencies are predicted using the 2-d.o.f. finite difference model (black line, hollow triangles), and at high frequencies using the 18-d.o.f. wave theoretical model (blue line, solid squares). The light dashed line is an interpolation.

Evidently, there is a low frequency pass-band, up to about 10 kHz, on which the attenuation is very close to zero. The fact that the decay results show a considerable amount of scatter there is a consequence of resonant effects in the finite difference model, since that model is finite. Since the attenuation is very low at those frequencies, nothing hinders the contribution from the end-reflections from interfering with the direct contribution from the source; thus, resonances develop. At some frequencies, the response point is at or near a resonant node, and a slight positive decay occurs; at other frequencies, it is at or near an antinode, and a slight negative decay (i.e., amplification) occurs. However, the interpretation is that there is almost no attenuation at those frequencies. Above about 4 kHz, there is a steep rise in the attenuation, indicating the beginning of a stop band. Were it continued above 20 kHz, the 2-d.o.f. finite difference would predict that stop band to extend to infinity along the frequency axis, a consequence of accounting for only two low modes (vertical and rotational oscillations of the tube against the fin stiffnesses).

The same stop band is also seen at 30 kHz in the wave model. The rest of the spectrum is dominantly a stop band, with decay in the range 1 – 2 dB per unit, but with narrow passbands occurring at 40 kHz, about 130 - 140 kHz, and about 160 kHz. This suggests that leakage monitoring could be concentrated on those frequency bands, since the leak-induced noise is least attenuated there.

The location of the minima are likely explainable by resonances within the repeating unit, and of the maxima by anti-resonances and by coincidence frequencies (at which there is a narrow peak in the radiation damping effect). The coincidence frequencies are at 57 kHz (smelt-fin), 130 kHz (smelt-tube), and 150 kHz (water-tube); there are, in fact, attenuation maxima at the first and third of these.

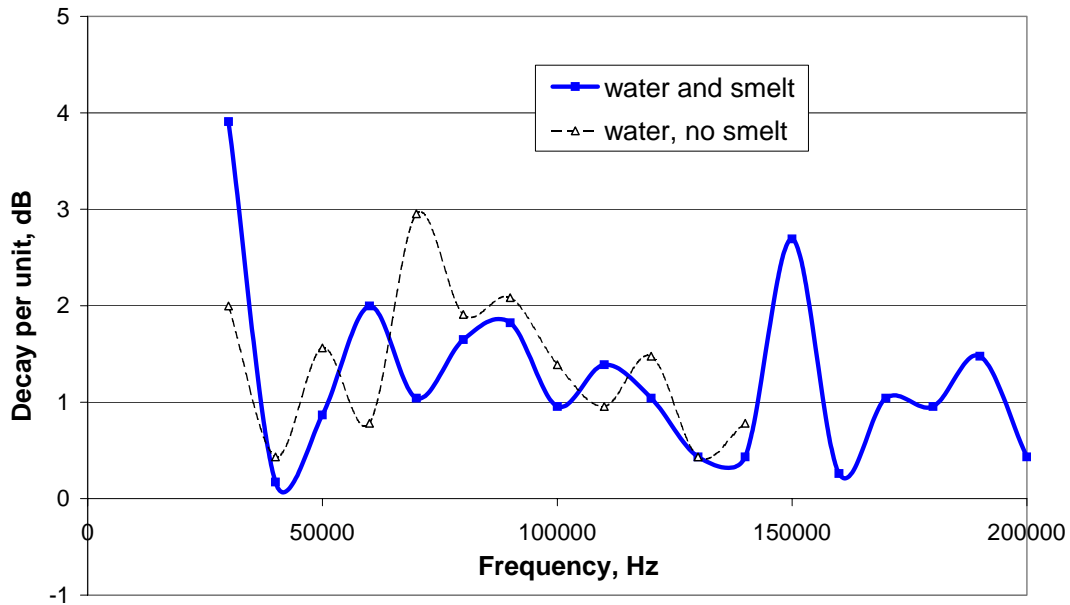


Figure 8. Effect of the smelt on the predicted attenuation across the pipes.

Figure 8 presents a comparison of the decay in the operating boiler (with smelt) to the same boiler not yet operated (without smelt). Notably, maxima and minima are slightly shifted because of the higher added mass of the smelt below 130 kHz.

2.2 Experimental verification

2.2.1 Measurement arrangements

Measurements were performed at Skoghall, Sweden, at 4.-5.5.2005 by Järvinen & Hildebrand. Measurements were focused to the bottom wall of the recovery boiler; see the figure below. The used AE-sensors were broadband ones, Fuji 1045S, and the data acquisition was performed by Wavebook 512 at 500 kHz sampling rates.



Figure 9. Measurements were performed at the bottom wall of the recovery boiler (left). Zoomed view at right.

Measurement direction was chosen as perpendicular to the pipe direction. That is, because the sound propagation in that direction clearly is more difficult and thus gets more decay. The excitation was supplied to the reference pipe. Excitation was generated by Nielson lead break test, sandpaper, breaking multiple leads simultaneously and a tiny metal-to-metal impact. Each of those excitation sources has own advantages depending on the frequency range and/or the distance of reference and response. That is taken into account in data-analysis by choosing the best available measurement for each of the spectral lines.

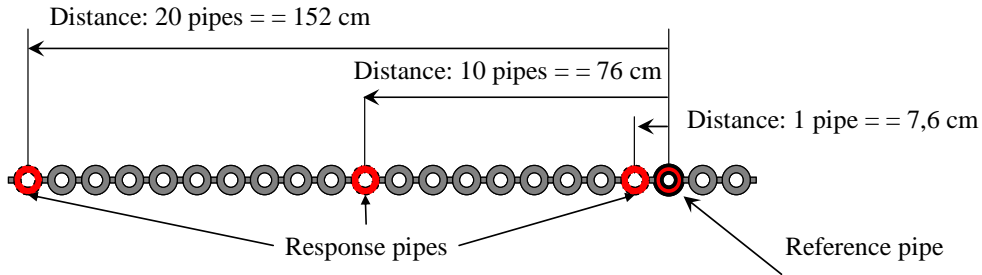


Figure 10. Principle of the measurement arrangement.

2.2.2 Noise consideration

Because of the partially weak response levels, the analysis was firstly focused to the determination of noise levels of the measurement arrangement. The figure below presents the noise level of the reference channel 1 (blue points). Threshold values of the noise levels to the each of the channels were determined from their measured noise data by means of moving average and suitable coefficient; this is drawn as solid red line. This level will be a guideline in later data-analysis. Noise is assumed to be as random and may freely vary below the defined threshold values.

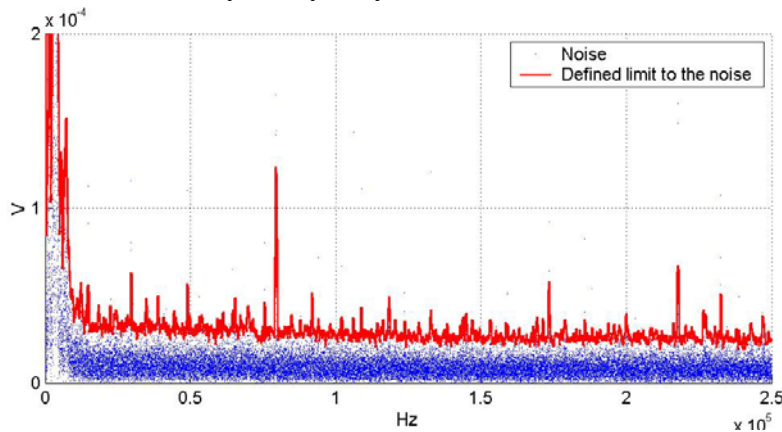


Figure 11. Determination of the threshold value of the noise level by means of moving average.

2.2.3 Optimization

In order to optimize the signal to noise ratios (STN) of measurements, Δ_1 , Δ_2 and Δ_3 were determined for each of the measurements to describe the STN ratios of references, responses and their noises. The figure below represents the choice of those deltas;

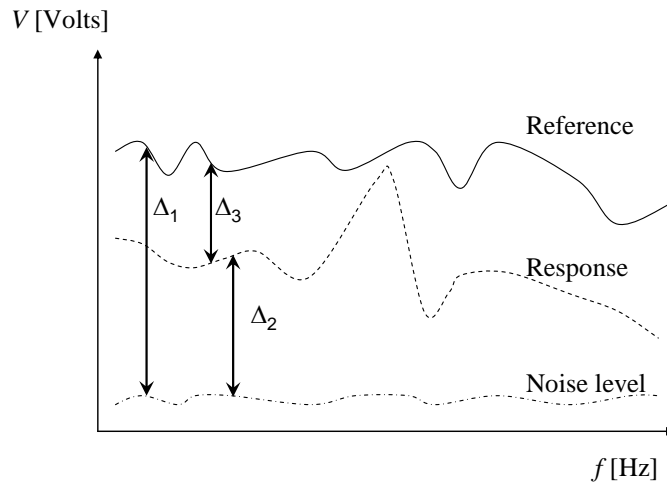


Figure 12. Determination of deltas for describing the STN ratios of references, responses and noise levels.

The first step in the optimization procedure is to read all the measurements as one matrix. After that they are handled systemically by means of two rules namely, Rule 1; Δ_1 must be over 6 dB, Rule 2: Δ_1 must be over 0 dB. Since the specific spectral lines of some measurements fulfils those rules, the next phase is to maximize the ratios Δ_1 , Δ_2 and Δ_3 . In the final results, each spectral line has chosen by using the maximum value of the combined STN –ratios, from the group of all the measurements. The Matlab® - code is added as Appendix C to the report.

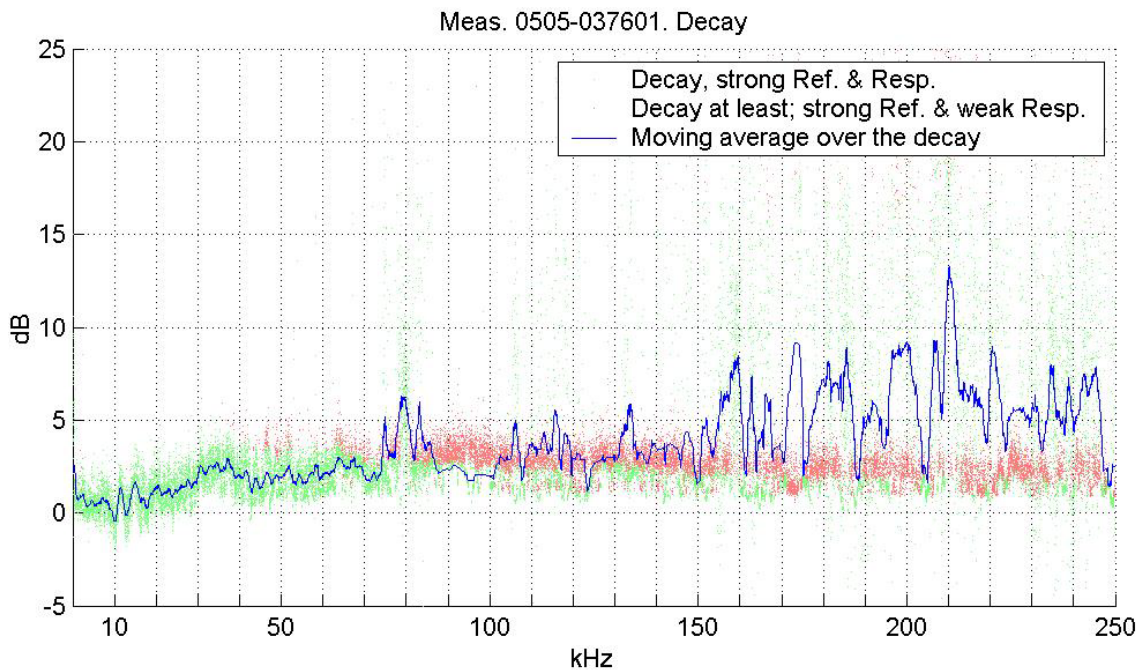


Figure 13. Experimental result of decay per unit, in function of frequency.

In the above figure, the green dots are drawn to the spectral lines, in which both the reference and response has been overhead of the defined noise threshold values. The red points means that the reference has been clearly over the noise level but response has been in the noise level. Thus, the red points presents the minimum decay values for the frequency lines they are drawn. Solid blue line is calculated by moving average through the green points.

One can observe from the figure, that under 20 kHz there is a range in which the negative attenuation, i.e. amplification is presented. After that range, namely 70...90 kHz, the strong stop

band is noticed. Beginning from about 100 kHz, what the higher the frequency is the higher attenuation levels are found. Moreover, the amount of high attenuation peaks / frequency is rapidly increasing. However, there are found some very narrow pass bands over the higher frequency range. In theory, the sound / vibration can propagate by using those few pass bands, but the energy content of the original signal is rapidly loosen.

Referring to the results of the theoretical study (figures 7 and 8), it can be concluded that the results are correlated quite a well. The base level of the attenuation is below 2 dB in theoretical and that same it is also in experimental study, up to 150 kHz. Add to this, the theoretical 2 DOF model predicted strong pass bands to the range of 0...20 kHz and that is true also in experimental model. Furthermore, both models are proposing the larger pass band to the just before 50 kHz and, around 70 kHz, the strong stop band is arising.

3 Steam leaks into the furnace

The relevant question is the size of steam leaks that one might expect to be able to detect using microphones listening to the noise inside the boiler (via tubular waveguides), and also the frequency bands that are relevant to monitoring. We give this topic less attention, so as to concentrate on the bottom wall, but a brief theoretical discussion is nevertheless provided.

According to the theory of Lighthill, a free jet acts like a quadropole. A quadropole source emits acoustic power, which is proportional to the cross-sectional area of the hole (diameter d), and the eighth power of the mean flow velocity U ,

$$\overline{W}_q \propto d^2 U^8. \quad (3.1)$$

The resulting spectrum is a broad-banded noise, centered around the Strouhal frequency

$$f_s = U / d. \quad (3.2)$$

A reasonable assumption is that the sound field in the boiler is dominated by the diffuse field, which tends to be the case in an environment with hard walls, hard reflectors / scatterers (such as pipes), and relatively large dimensions (in wavelengths), such as the inside of the boiler. For a diffuse sound field, the squared rms-pressure \tilde{p}^2 is given by

$$\tilde{p}^2 = \overline{W}_{source} + 10 \log \frac{4}{A'}, \quad (3.3)$$

where A' is the “room constant”, a measure of the net sound absorptivity of the surfaces of the enclosed space (in this case, the inside of the boiler).

The sound from a steam leak in boiler is thus estimated to be

$$\tilde{p}^2 = K d^2 U^8 + 10 \log \frac{4}{A'}. \quad (3.4)$$

The constant K is best estimated from published results of actual steam leaks, since it has not been possible in this project to measure an actual steam leak into a boiler (and it is not clear how K could be extrapolated or scaled from other gases, such as air, leaking into environments other than the hot flue gas environment of the recovery boiler). Defining a difference Δ between the sound pressure level L_p at some monitoring microphone point due to a steam leak, and that due to operational noise $L_{p,bkgd}$,

$$\Delta = L_p - L_{p,bkgd} = C + 20 \log d + 80 \log U + 10 \log \frac{4}{A'} - L_{p,bkgd} \quad (3.5)$$

where $C = 10 \log K$. From gas dynamics, it is known that U is insensitive to d in turbulent flow, so that

$$\Delta = C_2 + 20 \log d \quad (3.6)$$

where $C_2 = C + 80 \log U + 10 \log \frac{4}{A'} - L_{P,bkgd}$ is an unknown constant.

[Buckner & Paradis, 1990] simulated a leak using “an electronic driver powered by a white-noise generator, and an amplifier”; the signal generated was claimed to be representative of the sound from a leak of superheated steam in a recovery boiler through a $d = 3.2$ mm diameter hole, presumably at pressures and temperatures typical of an operating boiler. The plotted results of the sound level with and without the leak (the second representing, thus, background noise) show that the leak-induced sound field is typically about $\Delta = 10$ dB above the background noise level, by visual inspection, throughout a bandwidth of about 2 kHz. Hence,

$$C_2 = \Delta - 20 \log d = 1.9 \text{ dB}$$

is back calculated. A reasonable guess at a detectability criterion is that, to be detected by a monitoring system, sound at the microphone from a leak should probably rise at least $\Delta = 3$ dB above the background noise. That being so, then the smallest leak that would be heard under the same conditions as in [Buckner & Paradis, 1990] is

$$d = 10^{\frac{3.0-1.9}{20}} = 1.4 \text{ mm}$$

But, unfortunately, the Buckner & Paradis paper leaves many details unreported: microphone location with respect to the leak location, for the specific case for which results are plotted; the basis for the amplitude and frequency content of the simulation signal selected; etc. So, the result of the reasoning presented here is only that in a “typical boiler” (pressure, temperature), with a “typical” microphone position, the smallest hole detected would be about 1.4 mm. Moreover, that result relies completely on the electronically generated “simulated” leak signal having been truly representative of the actual sound that would have been generated by a 3.2 mm leak.

The reasoning used is more valuable than the result itself, because of the lack of unambiguous input information. Should more detailed results become available, the same reasoning could be applied to obtain a more reliable result.

Additionally, this work has included measurements of the sound pressure level inside the boiler at Rauma, while in operation. This was done with a tubular waveguide that entered the boiler through an access port near the black liquor spray nozzles. The orientation of the waveguide was slowly changed throughout the nearly 1 minute measurement interval (without any systematic angle – time dependence), in order to build a kind of average. Figure 9 shows these results in waterfall form, and figure 10 shows the overall level (on the bands 0-20 kHz and 5-20 kHz in the upper and lower curves, respectively) versus time.

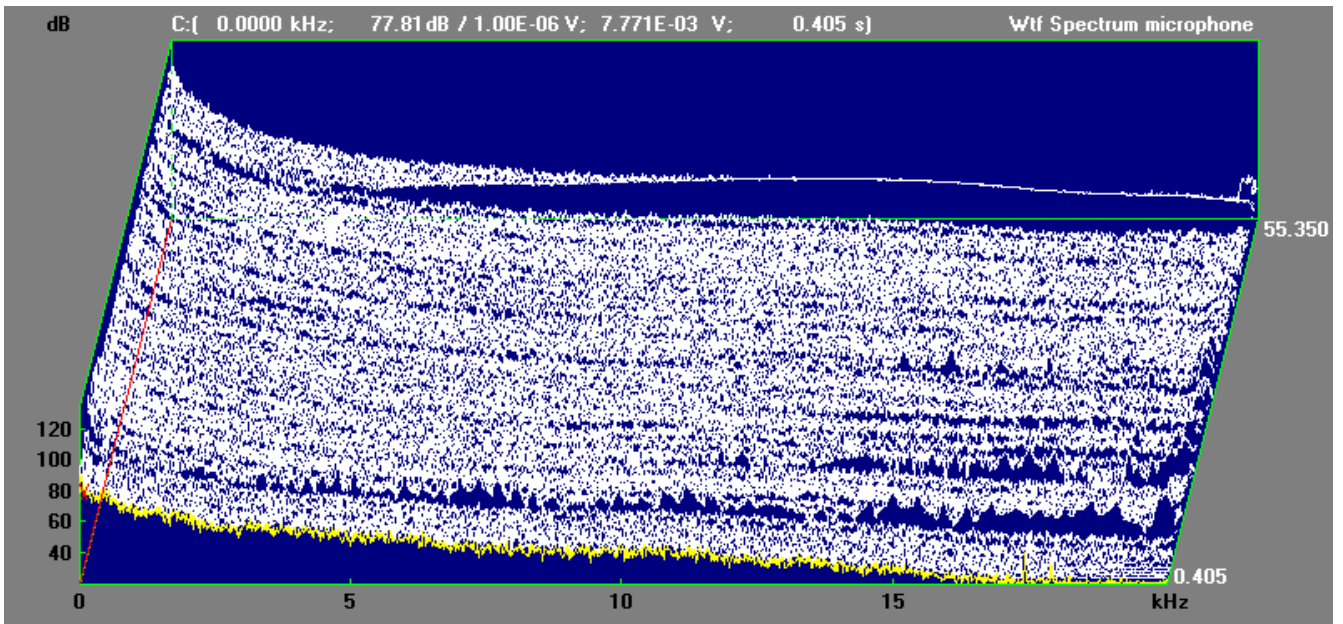


Figure 14. Sound pressure level inside the boiler.

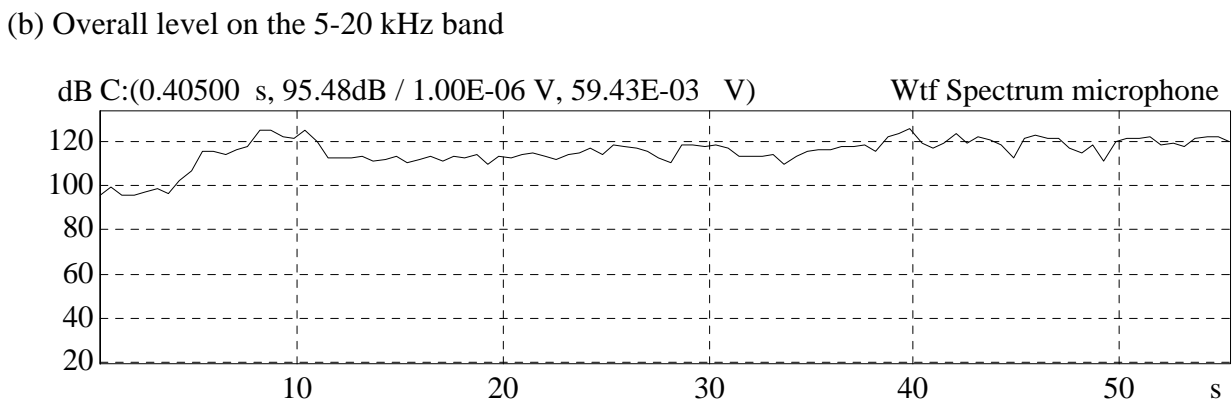
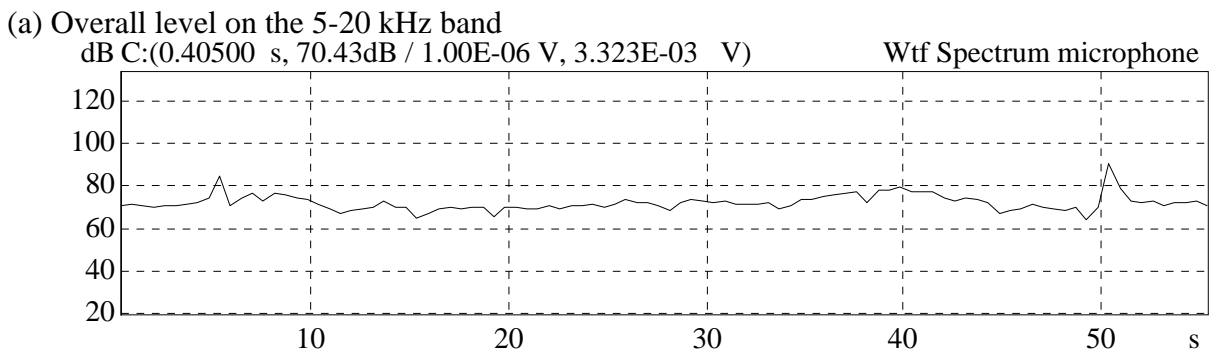


Figure 15. Overall sound pressure level inside the boiler, in (a) the 5-20 kHz band, and (b) the 0-20 kHz band.

These results could be used in combination with any new data that should become available on the sound power output from a leak, to give a new assessment of detectability versus hole size.

4 Conclusions

- High attenuation occurs across the pipes in the bottom wall, at the high frequencies typically monitored by acoustic emission transducers. This may result in a poor signal-to-noise ratio for water leaks that occur such that the nearest monitoring transducer is separated from the leak by several pipes. That situation risks making the leak very difficult to detect.
- However, there is reason to believe that certain narrow passbands do exist; these would be promising bands for monitoring. The current work does predict a few such bands (40 kHz, 135 kHz, 160 kHz), but uncertainties of the smelt properties make these predictions tenuous.
- Steam leaks down to 1.4 mm in the furnace can probably be detected, but with reservations about the published input data on which that conclusion is based. However, the logic presented to arrive at the conclusion would be useful should better input data become available.

The following are recommended as future research topics:

- An analytical study of the background noise from droplet expansion and combustion, in both the boiler interior (for steam leak monitoring) and in the bottom wall (for water leak monitoring). This is an interesting, but probably very difficult, thermo-acoustic problem. The drops probably act, acoustically, as a distribution of monopoles sources, since a volumetric expansion is the physical mechanism of a monopole source. However, the frequency content from each drop source will depend on the expansion rate or gas expulsion rate; thus, the droplet size distribution is an important factor. The monopoles radiate into the environment of the boiler, which can probably be characterized as a reverberant environment. Another aspect of this question is the sound-structure interaction at the bottom wall; i.e., how effectively does the droplet noise excite structure-borne sound in the bottom wall?

- A study of the mechanism for generation of sound by the leak (or developing leak). Is it...
 - metal cracking, or
 - turbulent fluid flow through a fissure, or
 - localized chemical reaction of the water with the smelt, or
 - localized rapid phase change of the water as it enters the smelt

that one should seek to monitor? What are the respective vibrational power inputs from each of these mechanisms into the bottom wall? Acoustic emission sensors are often successful in listening for cracking in structures. In the recovery boiler bottom wall, however, there is, in addition to the large attenuation across pipes, also the reservation that the corrosive type of deterioration may not give the same kind of energetic cracking as in other AE applications.

- Scale model or other measurement of **sound power** from a steam leak jet (490°C, 92 bar) into a hot environment (with sound speed similar to that in the boiler), knowing the hole diameter.

5 Bibliography

Adams, T (ed.) *Kraft Recovery Boilers*, TAPPI Press

Cremer,L., Heckl, M., and Ungar , E.E. (1988) *Structure Borne Sound: Structural Vibrations and Sound Radiation and Audio Frequencies*. 2nd ed., Springer-Verlag

Buckner and Paradis (1990) “Design and implementation of a commercial acoustic leak detection system for black liquor recovery boilers” *TAPPI Journal*, July 1990

Graff, K. (1975) *Wave Motion in Elastic Media*, ISBN 0-486-66745-6, Oxford University Press

Graff, K. (1970) “Elastic Wave Propagation in a Curved Sonic Transmission Line” *IEEE Transactions on Sonics and Ultrasonics*, vol. SU-17, No.1, January 1970, pp.1-6

Junger, M. and Feit, D. *Sound, Structures, and their Interaction*. ISBN 0-262-10034-7, Acoustical Society of America

Kawaji, M., Nikfarman, H., Tan, G., Grace, T.M. and Tran, H. *Thermal Properties for Recovery Boiler Char Beds* (publication and year unknown)

Appendix A: Fortran 77 code for the 18-d.o.f. wave theoretical model.

```

PROGRAM BLBOILER
C
C Structure-borne sound attenuation in bottom wall of
black liquor
C recovery boiler
C
C VERSION BB6: thick plate fin tube
C tube based on Graff's thick ring
theory
C corrections also effect long and
bending stiffness
C fluid loading below coincidence: as
added mass
C above coincidence: as
damping
C adjustable search for roots (in DO 70
loop)
C
COMPLEX
KBF, KBT, KLF, KLT, GMBF, GMNF, GMLF, GMBT, GMNT, GMLT, DF, DT, E
F, ET
COMPLEX A(18,18), G, AA(3,3)
COMPLEX CU, CI, CZ
COMPLEX
KBT0, KLT0, KBFO, KLF0, DF0, DT0, GMOD, TMA, TMB, TMC, ETEFF
REAL L, NUF, NUT
REAL KC, KSM, KW, KTRIAL, KTR0
LOGICAL DMIN, DMIN2
DIMENSION DTMT(150,150)
OPEN(UNIT=1, FILE='BB6.OUT')
CI=CMPLX(0.,1.)
CU=CMPLX(1.,0.)
CZ=CMPLX(0.,0.)
PI=3.141592653
C -----
C Input Properties
C geometric
HF=.004
L=.0127
HT=.00185
R=.0635/2.
C material
EFIN=2.1E+11
NUF=.3
RHOF=7800
ETAF=.01
ETUBE=2.1E+11
NUT=.3
RHOT=7800
ETAT=.01
C smelt
CSMELT=1400.
RHOSM=2000.
FQCT=0.
FQCF=0.
C water
CWATER=1500.
RHOW=1000.
FQCWT=0.
C
C -----
C ---MAIN LOOP---
C
DO 500 EFQ=4,5
DO 500 IFQ=1,9
FQ=IFQ*10.**EFQ
IF (FQ .LT. 30000.) GO TO 499
DO 500 IFQ=3,20
FQ=REAL(IFQ)*10000.
WRITE(*,*)INT(FQ), ' Hz'
OM=2.*PI*FQ
C -----
C
ICOINC=0
20 IF ((FQCT .GT. 0.) .OR. (FQCWT .GT. 0.)) THEN
REFFSM=0.
REFFW=0.
IF (FQCT .GT. 0.) REFFSM=1./SQRT(1.-FQCT/FQ)
IF (FQCWT .GT. 0.) REFFW=1./SQRT(1.-FQCWT/FQ)
ETAT=(RHOSM*CSMELT*REFFSM+RHOW*CWATER*REFFW)/(OM*RHOT
*HT)
ENDIF
IF (FQCF .GT. 0.) THEN
REFF=1./SQRT(1.-FQCF/FQ)
ETAF=RHOSM*CSMELT*REFF/(OM*RHOF*HF)
ENDIF
C
EF=CMPLX(EFIN,EFIN*ETAF)
ET=CMPLX(ETUBE,ETUBE*ETAT)
DF0=EF*HF*HF*HF/12./(1-NUF*NUF)
DT0=ET*HT*HT*HT/12./(1-NUT*NUT)
C
KBFO=CSQRT(CSQRT(OM*OM*RHOF*HF/DF0))
KLF0=OM*CSQRT(RHOF*(1-NUF*NUF)/EF)
KBT0=CSQRT(CSQRT(OM*OM*RHOT*HT/DT0))
KLT0=OM*CSQRT(RHOT*(1-NUT*NUT)/ET)
C
C Approximate thick-plate corrections (shear & rotary
inertia) for fin
TAU=.83
RGYR=HF/SQRT(12.)
GMOD=EF/2./(1+NUF)
TMA=DF0/RHOF/HF
TMB=-OM*OM*(RGYR*RGYR+DF0/GMOD/TAU/HF)
TMC=OM**4*RHOF*RGYR*RGYR/GMOD/TAU-OM*OM
KBF=CSQRT((-TMB+CSQRT(TMB*TMB-
4.*TMA*TMC))/2./TMA)
DF=DF0*(KBF0/KBF)**4
C
KLF=KLF0
C Approximate curvature, shear & rotary inertia
corrections for tube
C0=SQRT(ETUBE/RHOT/(1-NUT*NUT))
RGYR=HT/SQRT(12.)
GMOD=ET/2./(1+NUT)
TAU=.83
J0=0
DO 30 IK=100000,1,-1
KTRIAL=10.*KBT0*REAL(IK)/100000.
CALL THRING(OM,KTRIAL,RGYR,R,GMOD,TAU,C0,ET,AA)
CALL CDET(AA,CDAA)
IF (IK .LT. 3) GO TO 29
P1=(CD00-CD0)/CD0
P2=(CDAA-CD0)/CD0
IF ((P1 .GT. .01) .AND. (P2 .GT. .01)) THEN
J0=J0+1
IF (J0 .EQ. 2) KLT=KTR0
IF (J0 .EQ. 1) KBT=KTR0
ENDIF
29 CD00=CD0
CD0=CDAA
KTR0=KTRIAL
30 CONTINUE
DT=DT0*(KBT0/KBT)**4
ETEFF=ET*(KLT0/KLT)**2
C
C Smelt interaction correction
IF (ICOINC .EQ. 1) GO TO 40
IF (FQCT .EQ. 0.) THEN
KSM=OM/CSMELT
IF (KSM .GT. REAL(KBT)) THEN
FQCT=OFQ+(FQ-OFQ)*(KSM-RKBT0)/(REAL(KBT)-
RKBT0)
ICOINC=1
ELSE
FAC=SQRT(SQRT(1.+RHOSM/(RHOT*HT*SQRT(REAL(KBT)**2-
KSM*KSM))))
KBT=KBT*FAC
ENDIF
RKBT0=REAL(KBT)
ENDIF
C
IF (FQCF .EQ. 0.) THEN
KSM=OM/CSMELT
IF (KSM .GT. REAL(KBF)) THEN
FQCF=OFQ+(FQ-OFQ)*(KSM-RKBF0)/(REAL(KBF)-
RKBF0)
ICOINC=1
ELSE
FAC=SQRT(SQRT(1.+RHOSM/(RHOF*HF*SQRT(REAL(KBF)**2-
KSM*KSM))))
KBF=KBF*FAC
ENDIF

```

```

      RKBF0=REAL(KBF)
      ENDIF
C
      IF (FQCWT .EQ. 0.) THEN
        KW=OM/CWATER
        IF (KW .GT. REAL(KBT)) THEN
          FQCWT=OFQ+(FQ-OFQ)*(KW-RKBT0)/(REAL(KBT)-
RKBT0)
          ICOINC=1
          ELSE
            KBT=KBT*FAC
            ENDIF
            RKBT0=REAL(KBT)
            ENDIF
            IF (ICOINC .EQ. 1) GO TO 20
C
40     DIVIS=15.
50     IFOUND =0
        DO 70 IREG=1,150
        DO 70 IIMG=1,150
        G=CMPLX((REAL(IREG))/DIVIS,(REAL(IIMG)-
75.)/11.9)
        CALL
        COEFF(OM, HF, L, HT, R, EF, ETEFF, KBF, KBT, KLF, KLT, DF, DT, G, A
)
        CALL LOGDET(A, DETR)
        DTMT(IREG, IIMG)=DETR
70     CONTINUE
        IWRT=0
        DO 75 I=2,149
        IF (IWRT .EQ. 1) GO TO 75
        DO 74 J=2,149
        DTMT0=DTMT(I, J)
        IMIN=1
        DO 72 II=1,40
        DO 72 JJ=1,40
        IF (I-20+II .LT. 1) GO TO 72
        IF (J-20+JJ .LT. 1) GO TO 72
        IF (I-20+II .GT. 150) GO TO 72
        IF (J-20+JJ .GT. 150) GO TO 72
        DTMTC=DTMT(I-20+II, J-20+JJ)
        IF (DTMTC .LT. DTMT0) IMIN=0
72     CONTINUE
        DMIN=(IMIN .EQ. 1)
        DMIN2=((DMIN) .AND. (IWRT .EQ. 0))
        IF (DMIN) IWRT=1
        GRE=(REAL(I))/100.
        GIM=(REAL(J)-75.)/11.9
        ATTN=GRE
        ADIST=ATTN/(L+2.*R)
        DECAF=-20.*LOG10(EXP(-ATTN))
        DECDIS=-20.*LOG10(EXP(-ADIST))
C
      IF (DMIN2)
WRITE(1,*)FQ, ', ', DECAF, ', ', ETAF, ', ', ETAT, ', ', FQCF, ', ',
, F
C
      *QCT, ', ', FQCWT, ', ', J0, ', ', DIVIS
      IF (DMIN2) WRITE(1,*)FQ, ', ', DECAF, ', ', DIVIS
      IF (DMIN2) IFOUND=1
74     CONTINUE
75     CONTINUE
      IF (IFOUND .EQ. 0) THEN
        WRITE(*,*) 'ANOTHER PASS'
        DIVIS=DIVIS*10.
      ENDIF
      IF ((IFOUND .EQ. 0) .AND. (DIVIS .LE. 900000.))
GO TO 50
C
.....
.....
499 CONTINUE
      CLT=OM/REAL(KLT)
      CBT=OM/REAL(KBT)
      OFQ=FQ
500 CONTINUE
      END
C
C
C
*****
*****
      SUBROUTINE
      COEFF(OM, HF, L, HT, R, EF, ET, KBF, KBT, KLF, KLT, DF, DT, G, A)
C

```

```

      COMPLEX
      KBF, KBT, KLF, KLT, GMBF, GMNF, GMLF, GMBT, GMNT, GMLT, DF, DT, E
F, ET
      COMPLEX A(18,18), G
      COMPLEX CU, CI, CZ
      REAL L
      CI=CMPLX(0., 1.)
      CU=CMPLX(1., 0.)
      CZ=CMPLX(0., 0.)
      PI=3.141592653
C
      GMBF=CEXP(-CI*KBF*L)
      GMNF=CEXP(-KBF*L)
      GMLF=CEXP(-CI*KLF*L)
      GMBT=CEXP(-CI*KBT*PI*R)
      GMNT=CEXP(-KBT*PI*R)
      GMLT=CEXP(-CI*KLT*PI*R)
C
      DO 200 I=1,18
      DO 200 J=1,18
      A(I, J)=CZ
200 CONTINUE
C
      A(1,2)=CU
      A(1,3)=CU
      A(1,4)=CU
      A(1,11)=GMBF*EXP(-G)
      A(1,12)=GMNF*EXP(-G)
      A(1,13)=GMLT
C
      A(2,4)=CU
      A(2,7)=-CU
      A(2,13)=GMLT
      A(2,16)=-GMLT
C
      A(3,2)=GMBF*EXP(G)
      A(3,3)=GMNF*EXP(G)
      A(3,4)=-GMLT
      A(3,11)=CU
      A(3,12)=CU
      A(3,13)=-CU
C
      A(4,4)=GMLT
      A(4,7)=-GMLT
      A(4,13)=CU
      A(4,16)=-CU
C
      A(5,1)=CU
      A(5,5)=-CU
      A(5,6)=-CU
      A(5,10)=GMLF*EXP(-G)
      A(5,14)=-GMBT
      A(5,15)=-GMNT
C
      A(6,5)=CU
      A(6,6)=CU
      A(6,8)=-CU
      A(6,9)=-CU
      A(6,14)=GMBT
      A(6,15)=GMNT
      A(6,17)=-GMBT
      A(6,18)=-GMNT
C
      A(7,1)=GMLT*EXP(G)
      A(7,5)=GMBT
      A(7,6)=GMNT
      A(7,10)=CU
      A(7,14)=CU
      A(7,15)=CU
C
      A(8,5)=GMBT
      A(8,6)=GMNT
      A(8,8)=-GMBT
      A(8,9)=-GMNT
      A(8,14)=CU
      A(8,15)=CU
      A(8,17)=-CU
      A(8,18)=-CU
C
      A(9,2)=-CI*KBF
      A(9,3)=-KBF
      A(9,5)=-CI*KBT
      A(9,6)=-KBT
      A(9,11)=CI*KBF*GMBF*EXP(-G)
      A(9,12)=KBF*GMNF*EXP(-G)
      A(9,14)=CI*KBT*GMBT
      A(9,15)=KBT*GMNT
C

```

```

A(10,5)=CI*KBT
A(10,6)=KBT
A(10,8)=CI*KBT
A(10,9)=KBT
A(10,14)=-CI*KBT*GMBT
A(10,15)=-KBT*GMNT
A(10,17)=-CI*KBT*GMBT
A(10,18)=-KBT*GMNT
C
A(11,2)=-CI*KBF*GMBF*EXP(G)
A(11,3)=-KBF*GMNF*EXP(G)
A(11,5)=-CI*KBT*GMBT
A(11,6)=-KBT*GMNT
A(11,11)=CI*KBF
A(11,12)=KBF
A(11,14)=CI*KBT
A(11,15)=KBT
C
A(12,5)=CI*KBT*GMBT
A(12,6)=KBT*GMNT
A(12,8)=CI*KBT*GMBT
A(12,9)=KBT*GMNT
A(12,14)=-CI*KBT
A(12,15)=-KBT
A(12,17)=-CI*KBT
A(12,18)=-KBT
C
A(13,2)=-CI*KBF*KBF*KBF*DF
A(13,3)=KBF*KBF*KBF*DF
A(13,4)=-CI*KLT*ET*HT
A(13,7)=-CI*KLT*ET*HT
A(13,11)=-CI*KBF*KBF*KBF*DF*GMBF*EXP(-G)
A(13,12)=KBF*KBF*KBF*DF*GMNF*EXP(-G)
A(13,13)=CI*KLT*ET*HT*GMLT
A(13,16)=-CI*KLT*ET*HT*GMLT
C
A(14,2)=CI*KBF*KBF*KBF*DF*GMBF*EXP(G)
A(14,3)=-KBF*KBF*KBF*DF*GMNF*EXP(G)
A(14,4)=CI*KLT*ET*HT*GMLT
A(14,7)=CI*KLT*ET*HT*GMLT
A(14,11)=-CI*KBF*KBF*KBF*DF
A(14,12)=KBF*KBF*KBF*DF
A(14,13)=-CI*KLT*ET*HT
A(14,16)=-CI*KLT*ET*HT
C
A(15,1)=-CI*KLF*EF*HF
A(15,5)=-CI*KBT*KBT*KBT*DT
A(15,6)=KBT*KBT*KBT*DT
A(15,8)=-CI*KBT*KBT*KBT*DT
A(15,9)=KBT*KBT*KBT*DT
A(15,10)=CI*KLF*EF*HF*GMLF*EXP(-G)
A(15,14)=CI*KBT*KBT*KBT*DT*GMBT
A(15,15)=-KBT*KBT*KBT*DT*GMNT
A(15,17)=CI*KBT*KBT*KBT*DT*GMBT
A(15,18)=-KBT*KBT*KBT*DT*GMNT
C
A(16,1)=-CI*KLF*EF*HF*GMLF*EXP(G)
A(16,5)=-CI*KBT*KBT*KBT*DT*GMBT
A(16,6)=KBT*KBT*KBT*DT*GMNT
A(16,8)=-CI*KBT*KBT*KBT*DT*GMBT
A(16,9)=KBT*KBT*KBT*DT*GMNT
A(16,10)=CI*KLF*EF*HF
A(16,14)=CI*KBT*KBT*KBT*DT
A(16,15)=-KBT*KBT*KBT*DT
A(16,17)=CI*KBT*KBT*KBT*DT
A(16,18)=-KBT*KBT*KBT*DT
C
A(17,2)=-KBF*KBF*DF
A(17,3)=KBF*KBF*DF
A(17,5)=KBT*KBT*DT
A(17,6)=-KBT*KBT*DT
A(17,8)=-KBT*KBT*DT
A(17,9)=KBT*KBT*DT
A(17,11)=-KBF*KBF*DF*GMBF*EXP(-G)
A(17,12)=KBF*KBF*DF*GMNF*EXP(-G)
A(17,14)=KBT*KBT*DT*GMBT
A(17,15)=-KBT*KBT*DT*GMNT
A(17,17)=-KBT*KBT*DT*GMBT
A(17,18)=KBT*KBT*DT*GMNT
C
A(18,2)=-KBF*KBF*DF*GMBF*EXP(G)
A(18,3)=KBF*KBF*DF*GMNF*EXP(G)
A(18,5)=KBT*KBT*DT*GMBT
A(18,6)=-KBT*KBT*DT*GMNT
A(18,8)=-KBT*KBT*DT*GMBT
A(18,9)=KBT*KBT*DT*GMNT
A(18,11)=-KBF*KBF*DF
A(18,12)=KBF*KBF*DF
A(18,14)=KBT*KBT*DT
A(18,15)=-KBT*KBT*DT
A(18,17)=-KBT*KBT*DT
A(18,18)=KBT*KBT*DT
C
RETURN
END
C
C
*****
*****
SUBROUTINE LOGDET(A,DETR)
C Computes the natural logarithm of the determinant
of complex matrix A
COMPLEX A(18,18),AT(18,18),SW,MODF,FV,CU
M=18
CU=CMPLX(1.,0.)
MODF=CU
DETR=0
IP=0
DO 200 I=1,M
DO 200 J=1,M
AT(I,J)=A(I,J)
200 CONTINUE
205 IP=IP+1
DO 207 J=M,IP,-1
IF (CABS(AT(J,IP)) .GT. 1E-12) IFNZ=J
207 CONTINUE
IF (IFNZ .GT. IP) THEN
DO 209 J=1,M
SW=AT(IP,J)
AT(IP,J)=AT(IFNZ,J)
AT(IFNZ,J)=SW
209 CONTINUE
MODF=-MODF
ENDIF
FV=AT(IP,IP)
DO 210 J=IP,M
AT(IP,J)=AT(IP,J)/FV
210 CONTINUE
MODF=MODF/FV
DETR=DETR-LOG(CABS(FV))
DO 220 I=IP+1,M
FV=AT(I,IP)
DO 220 J=IP,M
AT(I,J)=AT(I,J)-FV*AT(IP,J)
220 CONTINUE
IF (IP .LT. M-1) GO TO 205
FACR=1.
DO 230 I=1,M
FACR=FACR*CABS(AT(I,I))
230 CONTINUE
DETR=DETR+LOG(FACR)
RETURN
END
C
C
*****
*****
SUBROUTINE
THRING(OM,KTRIAL,RGYR,R,G,TAU,C0,E,AA)
REAL KTRIAL,KR
COMPLEX AA(3,3),CI,E,G
CI=CMPLX(0.,1.)
C=OM/KTRIAL
C
ER=RGYR*KTRIAL
KR=RGYR/R
GR=TAU*G/E
CR2=C*C/C0/C0
C
AA(1,1)=-
(ER*ER+KR*KR*ER*ER+GR*KR*KR*(1.+KR*KR))-ER*ER*CR2)
AA(1,2)=CI*KR*ER*(1.+KR*KR+GR*(1.+KR*KR))
AA(1,3)=KR*(ER*ER+GR*(1.+KR*KR)+ER*ER*CR2)
C
AA(2,1)=-KR*(ER*ER+GR*(1.+KR*KR)+ER*ER*CR2)
AA(2,2)=CI*ER*(KR*KR+GR*(1.+KR*KR))
AA(2,3)=ER*ER+GR*(1.+KR*KR)-ER*ER*CR2
C
AA(3,1)=CI*KR*ER*(1.+KR*KR+GR*(1.+KR*KR))
AA(3,2)=KR*KR+KR**4+GR*(1.+KR*KR)*ER*ER-
ER*ER*CR2
AA(3,3)=-CI*ER*(KR*KR+GR*(1.+KR*KR))
C
RETURN
END
C

```

```
C
*****
*****
      SUBROUTINE CDET(A,CDETR)
C Computes the modulus of the determinant of complex
3X3 matrix A
      COMPLEX A(3,3),DETR,D1,D2,D3
      D1=A(2,2)*A(3,3)-A(3,2)*A(2,3)
      D2=A(2,1)*A(3,3)-A(3,1)*A(2,3)
      D3=A(2,1)*A(3,2)-A(3,1)*A(2,2)
      DETR=A(1,1)*D1-A(1,2)*D2+A(1,3)*D3
      CDETR=CABS(DETR)
      RETURN
      END
```

Appendix B: Fortran 77 code for the 2-d.o.f. finite difference model.

```

PROGRAM BOILER1b
C
C Analysis of structure-borne sound propagation in
C the bottom wall of a
C black-liquor recovery boiler, transverse to
C coolant-water tubes.
C
C version 1: * time-domain finite difference approach
C           * lumped element approximation of wall
C components:
C           - filled pipes rigid
C masses/rotational inertias
C           - fins as vertical and rotational
C springs
C           * damping not considered (from sludge,
C welds, etc)
C           * quasi-longitudinal waves not
C considered
C version 1b: same as version 1, except that the
C multiple runs are made
C           with a frequency loop; for ea freq
C step, tonal excitation
C           is given over a total time of 100 times
C the tonal period,
C           with a sampling frequency one-tenth of
C the excitation
C           frequency. The frequency response at
C the excitation freq
C           is found at the measurement points
C (integral of the prod-
C           uct of the response and a unit sine
C function, integral of
C           similar product with cos function -->
C norm of those two
C           integrals); from the amplitudes, a
C decay rate is found in
C           dB/repeating element. The frequency is
C stepped
C           logarithmically.
C
C   DIMENSION V(100),VOLD(100),VNEW(100)
C   DIMENSION TH(100),THOLD(100),THNEW(100)
C   REAL M,JROT,K,NU,LFIN
C
C   OPEN(UNIT=1,FILE='B1b.OUT')
C
C   PI=3.141592654
C
C           .....input
C parameters.....
C   E=2.1E+11
C   RHO=7800.
C   NU=.3
C   RHOWAT=1000.
C   TTUBE=.00185
C   TFIN=.004
C   LFIN=.0127
C   DIATUB=.0635
C
C   R=DIATUB/2.
C   DMOD=(E*TFIN**3)/(12.*(1.-NU*NU))
C
C           .....calculated structural
C parameters.....
C   M=2.*PI*R*TTUBE*RHO+PI*R*R*RHOWAT
C   JROT=2.*PI*R*R*TTUBE*RHO
C   K=12.*DMOD/LFIN**3
C   D=LFIN*LFIN/6.
C
C   WRITE(*,*)'filled tube mass M = ',M,' kg per
C m'
C   WRITE(*,*)'...rot inertia JROT = ',JROT,'
C kg*m^2 per m'
C   WRITE(*,*)'fin stiffness K = ',K,' N/m per
C m'
C   WRITE(*,*)'fin offset dist D = ',D,' m'
C
C           .....measurement
C parameters.....
C excitation freq FQ, computational time step DT,
C total time TSTOP,
C first measurement element MEAS1, second measurement
C element MEAS2
C   WRITE(*,*)' EXC FREQ, TIME STEP 1, ACTUAL TIME
C STEP, TOT TIME'
C   DO 400 IFQEXP=2,5
C   DO 400 IFQFAC=1,9
C   FQ=REAL(IFQFAC)*10**IFQEXP
C   DT0=.00001
C   DT1=1./(10.*FQ)
C   DT=DT1
C   IF (DT .GT. DT0) DT=DT0
C   TSTOP=100./FQ
C   WRITE(*,*)FQ,' Hz','DT1,' s','DT,' s','TSTOP,'
C s'
C   MEAS1=2
C   MEAS2=40
C   F1=(K*DT*DT/M)
C   F2=(K*D*DT*DT/JROT/2.)
C   WRITE(*,*)F1,F2
C   ISCN=10000
C   IWRITE=1
C
C           .....initial
C conditions.....
C   IW=0
C   ISC=0
C   WRITE(*,*)' '
C   WRITE(*,*)'running...'
C   AMPL1A=0.
C   AMPL1B=0.
C   AMPL2A=0.
C   AMPL2B=0.
C   DO 50 J=1,100
C   V(J)=0.
C   VOLD(J)=0.
C   TH(J)=0.
C   THOLD(J)=0.
C   50 CONTINUE
C
C           .....system
C response.....
C   T=0.
C   100 T=T+DT
C   VNEW(1)=0.
C   VNEW(100)=0.
C   THNEW(1)=SIN(2.*PI*FQ*T)
C   THNEW(100)=0.
C   DO 200 J=2,99
C   C1=2.*V(J)-V(J-1)-V(J+1)+(D/2.)*TH(J+1)-
C (D/2.)*TH(J-1)
C   VNEW(J)=2.*V(J)-VOLD(J)-(K*DT*DT/M)*C1
C   C2=D*TH(J)+V(J-1)-
C V(J+1)+(D/2.)*TH(J+1)+(D/2.)*TH(J-1)
C   THNEW(J)=2.*TH(J)-THOLD(J)-
C (K*D*DT*DT/JROT/2.)*C2
C   200 CONTINUE
C
C   AMPL1A=AMPL1A+SIN(2.*PI*FQ*T)*VNEW(MEAS1)
C   AMPL1B=AMPL1B+COS(2.*PI*FQ*T)*VNEW(MEAS1)
C   AMPL2A=AMPL2A+SIN(2.*PI*FQ*T)*VNEW(MEAS2)
C   AMPL2B=AMPL2B+COS(2.*PI*FQ*T)*VNEW(MEAS2)
C
C   IW=IW+1
C   IF (IW .EQ. IWRITE) THEN
C   WRITE(1,*)T,' ',VNEW(MEAS1),' ',THNEW(MEAS1),' ',VNEW
C (MEAS2),' ',
C   *THNEW(MEAS2)
C   IW=0
C   ENDIF
C   ISC=ISC+1
C   IF (ISC .EQ. ISCN) THEN
C   WRITE(*,*)T,' s'
C   ISC=0
C   ENDIF
C
C   DO 250 J=1,100
C   VOLD(J)=V(J)
C   THOLD(J)=TH(J)
C   V(J)=VNEW(J)
C   TH(J)=THNEW(J)

```

```
250 CONTINUE
  IF (T .LT. TSTOP) GO TO 100
  AMPL1=SQRT(AMPL1A*AMPL1A+AMPL1B*AMPL1B)
  AMPL2=SQRT(AMPL2A*AMPL2A+AMPL2B*AMPL2B)
  AELEM=(-1./(MEAS2-MEAS1))*LOG(AMPL2/AMPL1)
  ADIST=AELEM/(LFIN+2.*R)
  DECAY=-20.*LOG10(EXP(-AELEM))

WRITE(1,*)FQ, ', ', DECAY, ', ', AMPL1, ', ', AMPL2, ', ', AELEM,
', ', ADIST
  WRITE(*,*)'          DECAY=', DECAY, 'dB'
400 CONTINUE
  END
```

Appendix C: Matlab® code for the Skoghall measurements

```
% Projekti Sooda, Skoghallin mittaukset
%
% Tämä file avaa kaikki mittaustulokset sekä etsii
% etsii parhaan mittauksen jokaiselle yksittäiselle spektriviivalle.
%
% Kuitenkin, jos ehtoja koskien STN-suhdetta ei läpäistä,
% k.o. spektriviivalle ei tulosteta mitään.
%
% Tuloksena on kuva värähtelyn vaimenemisesta taajuuden
% funktiona,
% tulos on normalisoitu yhdelle putkipoikkileikkaukselle.
%
%
% Author Ville Jarvinen 05/2005
%
%
clear all, close all

% Measurement directory
path = 'C:\Ville\Sooda\mittaus\Skoghall\data\Matlab\';

% Define noise levels
noise = load([path,'0405_009t']);
[fd1,f] = oma_fft_data(noise.ch(1).data,5e5);
fd2 = oma_fft_data(noise.ch(2).data,5e5);
nl1 = 3*oma_ma(abs(fd1),55);
nl2 = 3*oma_ma(abs(fd2),55);
% figure(11),clf, grid on
% line_1 = line(f,abs(fd1),'Color','b');
% line_2 = line(f,nl1,'Color','r');
clear noise

% intialisation of calculator
calc = 0;

% for loop to load all the measurements
for k = 1:2;

    if k==1,
        date = '0405';
        file_nos = [0:8 11:16];
    else
        date = '0505';
        file_nos = [1:13];
    end

    for i = file_nos;
        % Load the data
        if i<10,
            fname = [path,date, '_00', num2str(i) ,'.t']; else,
            fname = [path,date, '_0', num2str(i) ,'.t'];
        end
        data = load(fname);

        % Factor means the number of pipe cross_sections, over which
        % the current measurement is performed
        if strcmp(date,'0405')
            if i<9
                factor = 20;
            else
                factor = 1;
            end
        else
            factor = 10;
        end

        % FFT for data
        fd1 = abs( oma_fft_data(data.ch(1).data,5e5) );
        fd2 = abs( oma_fft_data(data.ch(2).data,5e5) );

        % Increase the calculator value by 1
        calc = calc+1;

        % Calculate the ratios; r1 is ref./noise, r2 is resp./noise, r3 is
        % ref/resp.
        r1 = fd1./nl1;
        r2 = fd2./nl2;
        r3 = fd1./fd2;

        % Create the matrices for all the measurements
        FACTOR(calc,1) = factor;
        % DELTA changes ratios to dB-scale
        DELTA1(calc,:) = 20*log10(r1);
        DELTA2(calc,:) = 20*log10(r2);
        DELTA3(calc,:) = 20*log10(r3);

        % Save spectral datas
        d1(calc,:) = fd1;
        d2(calc,:) = fd2;

        % figure(calc); clf, grid on
        % set(gcf,'position',[300+10*i 400+10*i 700 400])
        % title(['Meas. ',date, '-0', num2str(i),
        % Decay']),xlabel('Hz'),ylabel('dB')
        % line(f, DELTA1, 'color', 'r','linestyle','-','marker',
        % 'none','markersize',2.2);
        end
    end

    % Maximization of STN -ratio
    %=====
    % Rule 1; signal to noise ratio for reference must be good enough (in
    % dB:s)

    rule_1 = DELTA1 >=6;
    rule_2 = DELTA2 >=0;

    % [D2_min, D2_min_index] = min(DELTA2);
    % Maximize the DELTA3 + DELTA2
    [D3_max, D3_max_index] = max(DELTA2 + DELTA3 +
    DELTA1);

    % Selection of data points, according to the rule_1 and max. of sum
    % of DELTAS
    DECAFY = zeros(1,length(fd1));
    factors = zeros(1,length(fd1));

    for i=1:length(fd1)
        mi3 = D3_max_index(i);
        if rule_1(mi3,i)==1 & rule_2(mi3,i)==1
            data_ref = d1(mi3,i);
            data_resp = d2(mi3,i);
            DECAFY(i) = (20*log10(data_ref/data_resp) )/ FACTOR(mi3);
            factors(1,i)=FACTOR(mi3);
        else
            DECAFY(i) = 0;
        end
    end

    DECAFY2 = zeros(1,length(fd1));
    factors2 = zeros(1,length(fd1));

    for i=1:length(fd1)
        mi3 = D3_max_index(i);
        if rule_1(mi3,i)==1 & rule_2(mi3,i)==0
            data_ref = d1(mi3,i);
            data_resp = d2(mi3,i);
            DECAFY2(i) = (20*log10(data_ref/data_resp) )/ FACTOR(mi3);
            factors2(1,i)=FACTOR(mi3);
        else
            DECAFY2(i) = 0;
        end
    end
end
```

```

        DECA2(i) = 0;
    end
end

% ind separates the good data points, bad ones will not be drawn at
all
ind = DECA2 ~= 0;
ind2 = DECA22 ~= 0;
figure(88), grid on, plot(f(ind), D3_max_index(ind), 'ro'), grid on
set(gcf, 'position', [200 50 700 600])
% Figure
figure(89); clf, grid on
set(gcf, 'position', [500 350 700 600], 'visible', 'on')
set(gca, 'xlim', [0 250e3], 'ylim', [-5 25])
set(gca, 'XTickLabelMode', 'manual', 'xtick', [1:25]*1e4, 'xticklabel', '10|
||50|||100|||150|||200|||250')
title(['Meas. ', date, '-0', num2str(i),
Decay']), xlabel('kHz'), ylabel('dB')
line(f(ind), DECA2(ind), 'color', [1 1 .5], 'linestyle', 'none', 'marker',
',', 'markersize', 2.2);
line(f(ind2), DECA22(ind2), 'color', [1 .5 .5], 'linestyle', 'none',
'marker', ',', 'markersize', 2.2);
line(f(ind), oma_ma(DECA2(ind), 133), 'color', [0 0 1], 'linestyle', '-',
'marker', 'none', 'markersize', 2.2);

leg=legend('Decay, strong Ref. & Resp.', 'Decay at least; strong Ref.
& weak Resp.', 'Moving average over the decay');

% Save the figure in jpg.format
set(gcf, 'PaperUnits', 'centimeters', 'Papertype', 'A4', 'PaperOrientation', 'p
orrait', 'Paperposition', [0, 3 0.3 17 10.0])
spath='C:\Ville\Sooda\mittaus\Skoghall\figs';
figure(calc), saveas(gcf, [spath '\000kuva_optimal', num2str(i), '.jpg'])
set(gcf, 'visible', 'on');

%
% Lukee kaikki mittausfilet
%
% function read_all_files
%
%
%
%
%
clear all, close all

rms = 1;
file_ind = 1:16;
lpath = 'C:\Ville\Sooda\mittaus\Skoghall\Data\wav\0405_0';
spath = 'C:\Ville\Sooda\mittaus\Skoghall\Data\Matlab\0405_0';

for i = file_ind
    if i < 10,
        fname = [lpath, '0', num2str(i), '.wav'];
    else, fname = [lpath, num2str(i), '.wav'];
    end
    [y, sr, NBITS] = wavread(fname);
    tmax = length(y)/sr;
    Index = 1:tmax/(1/sr);
    size_data = size(y);
    for k = 1:size_data(2);
        ch(1).name = 'ch_1'; ch(1).Input = 5; ch(1).Scale = 1;
        ch(2).name = 'ch_2'; ch(2).Input = 5; ch(2).Scale = 1;
        ch(k).data = (y(Index, k) * ch(k).Input * rms * ch(k).Scale);
    end

    if i < 10, save([spath, '0', num2str(i), 't', '.mat'], 'ch'), else,
        save([spath, num2str(i), 't', '.mat'], 'ch'), end
end

if strcmp(fname(end-8:end), '5_009.wav')
    for i = 1:size_data(2);
        ch(i).noise = (y(Index, i) * ch(i).Input * rms * ch(i).Scale);
    end
else

```

```

        for i = 1:size_data(2);
            ch(i).data = (y(Index, i) * ch(i).Input * rms * ch(i).Scale);
        end
    end
end

% FUNCTION Moving Average
function out = oma_ma(data, bb)
%
%
%
% Moving Average
%
% inputs:
% data: data to be averaged
% bb: number of data points to be used in averaging process
%
%
% Author: Ville Järvinen
%

D = zeros(bb, length(data));
for a = 1:bb
    if a == 1
        v = [];
        D(a,:) = [data(:, a:end), v];
    else
        v = ones(1, a-1) .* data(end-a+1 :); % OR: v = ones(1, a-1) .*
data(end-1 : -1: end-a+1);
        D(a,:) = [data(:, a:end), v];
    end
end
md = mean(D);
shift = floor(bb/2);

out = [md(1) * ones(1, shift) md(1:end-shift)];

```